

國立交通大學

電信工程學系

碩士論文

多輸入/輸出正交分頻多工與多輸入/輸出多載波分  
碼多重進接系統之電腦模擬與效能鑑定



Computer Simulation and Performance Evaluation  
on Cellular MIMO-OFDM and MIMO MC-CDMA  
Systems

研究生：鄒鎧駿

指導教授：黃家齊 博士

中華民國九十六年七月

多輸入/輸出正交分頻多工與多輸入/輸出多載波分  
碼多重進接系統之電腦模擬與效能鑑定  
Computer Simulation and Performance Evaluation  
on Cellular MIMO-OFDM and MIMO MC-CDMA  
Systems

研究生：鄒鎧駿

Student : Kai-Chun Chou

指導教授：黃家齊

Advisor : Dr. Chia-Chi Huang



A Thesis

Submitted to Department of Communication Engineering  
College of Electrical and Computer Engineering  
National Chiao Tung University  
in Partial Fulfillment of the Requirements  
for the Degree of  
Master of Science  
in  
Communication Engineering  
July 2007  
Hsinchu, Taiwan, Republic of China

中華民國九十六年七月

# 多輸入/輸出正交分頻多工與多輸入/輸出多載波分 碼多重進接系統之電腦模擬與效能鑑定

學生：鄒鎧駿

指導教授：黃家齊

國立交通大學電信工程學系 碩士班



這篇論文使用電腦模擬來評估以正交分頻多工為基礎的蜂巢系統。模擬的系統應用空間多重傳輸來增加頻譜使用效率。對於多輸入/輸出正交分頻多工系統，我們模擬一個經過改良的 V-BLAST 偵測技術和迴旋編碼的通訊系統。至於多輸入/輸出多載波分碼多重進接系統，我們使用一種遞迴式多層級偵測技術。我們使用一種簡單的適應性最小平均平方誤差等化器和層級式天線干擾消除概念來減輕天線間的相互干擾並得到初始的資料偵測。接著藉由多路徑干擾消除技術達到空間分集及多重路徑分集的目的。我們也對這兩種系統的錯誤率效能以及複雜度做分析比較。模擬結果顯示在高訊號雜訊比時多輸入/輸出正交分頻多工系統有較好的表現，而在低訊號雜訊比時則是多輸入/輸出多載波分碼多重進接系統表現較佳。以行動台的所在位置來考量路徑損失和遮蔽衰減，模擬系統所處的蜂巢環境。運用電腦模擬來計算訊號干擾比的分佈。我們也驗證了用高斯訊號模擬干擾訊號的可靠性。

# Computer Simulation and Performance Evaluation on Cellular MIMO-OFDM and MIMO MC-CDMA Systems

Student : Kai-Chun Chou

Advisor : Dr. Chia-Chi Huang

Department of Communication Engineering  
National Chiao Tung University

## ABSTRACT

This paper addresses cellular systems based on orthogonal frequency division multiplexing (OFDM). The simulated systems apply spatial multiplexing to increase spectral efficiency. For MIMO-OFDM system, we simulate a communication system based on modified V-BLAST detections and convolutional encoding. For MIMO MC-CDMA systems, we use a multi-layered detection method. We use a simple adaptive MMSE equalizer followed by a layered antenna interference cancellation technique to suppress the inter-antenna interference and obtain initial decision results. Afterwards, a multipath interference cancellation is exploited to fully achieve both spatial diversity and multipath diversity. We also investigate and compare the error performances and complexity of these two systems. Simulation results show that MIMO-OFDM systems have better performance at high SNR while MIMO MC-CDMA systems perform better at low SNR. The systems are then situated in a cellular structure whereas the cellular environment model takes into account path loss and shadowing depending on the position of the mobile station. Computer simulations are used to calculate the distributions of signal-to-noise ratio. We also show that the Gaussian approximation for interference signals is an appropriate assumption.

## 誌謝

首先感謝指導教授黃家齊博士在專業領域與生活處事上對我的諄諄教誨，使我在這兩年中獲益良多。同時要感謝陳紹基教授和吳文榕教授的建議與指導，使我的論文能更為完整。

感謝古孟霖學長的熱心指導，不厭其煩地解答我課業上的疑問，並指引我研究的方向，使我得以順利完成碩士研究；感謝實驗室同學邱麟凱對工作站的架設與維護，讓我能夠跑完電腦模擬；感謝研究所期間所有幫助過我的老師、學長姐及同學們。



最後更要感謝我的家人，爸爸、媽媽及妹妹在我求學路上的鼓勵與支持，也要感謝一直在我身邊鼓勵我的女友。因為有他們，我才能順利完成碩士學位。

# Contents

<b>Chapter 1 Introduction.....</b>	<b>1</b>
1.1 MIMO-OFDM .....	2
1.2 MIMO MC-CDMA.....	3
1.3 About The Thesis .....	4
<b>Chapter 2 System Model .....</b>	<b>5</b>
2.1 MIMO-OFDM .....	5
2.2 MIMO MC-CDMA.....	6
<b>Chapter 3 Detection Methods for MIMO-OFDM and MIMO MC-CDMA Systems....</b>	<b>9</b>
3.1 V-BLAST Detection Methods for MIMO-OFDM Systems .....	10
3.2 Iterative Multi-layered Detection Methods for MIMO MC-CDMA Systems .....	12
3.2.1 Layered Antenna Interference Cancellation and Adaptive MMSE Equalization .....	13
3.2.2 Multipath Interference Cancellation .....	14
3.2.3 Iterative Multi-layered Detection.....	16
<b>Chapter 4 Multi-cell Environment.....</b>	<b>20</b>
4.1 Propagation Loss Model .....	20
4.2 Distributions of Signal-to-Noise Ratio .....	21
4.3 Cellular Interference Modeling.....	27
4.3.1 Gaussian Approximation .....	28
<b>Chapter 5 Simulation Results .....</b>	<b>30</b>
5.1 Simulation Environments.....	30
5.2 The Performance of MIMO-OFDM System.....	33
5.3 The Performance of MIMO MC-CDMA System.....	37
5.4 Comparison of the MIMO-OFDM and MIMO MC-CDMA systems .....	46
5.5 Multi-cell Environment.....	49
5.5.1 Gaussian Approximation.....	49
5.5.2 Analyses of System Performance in Multi-cell Environment .....	52
<b>Chapter 6 Conclusions.....</b>	<b>54</b>
<b>APPENDIX A The Modified MMSE V-BLAST Equalizer .....</b>	<b>56</b>
<b>Reference .....</b>	<b>58</b>

# List of Tables

Table 5.1: Simulation parameters common for both MIMO-OFDM and MIMO MC-CDMA systems.....	32
Table 5.2: Simulation parameters for MIMO-OFDM system.....	32
Table 5.3: Rate 1/2 maximum free distance codes.....	33
Table 5.4: Simulation parameters for MIMO MC-CDMA system.....	33
Table 5.5: The complexity comparison of MIMO-OFDM and MIMO MC-CDMA system.....	47



# List of Figures

Figure 2.1: The transmitter block diagram of the MIMO-OFDM system.....	6
Figure 2.2: The transmitter block diagram of the MIMO MC-CDMA system .....	6
Figure 2.3: The MC-CDMA transmit scheme at the $m$ th transmit antenna.....	8
Figure 3.1: The receiver block diagram of the MIMO-OFDM system .....	12
Figure 3.2: The first iteration of the multi-layered detection method.....	18
Figure 3.3: The second and latter iterations of the multi-layered detection method.....	19
Figure 4.1: Simulated distribution of Downlink SIR.....	25
Figure 4.2: Initial portion of Figure 4.2 .....	25
Figure 4.3: Simulated distribution of Uplink SIR.....	26
Figure 4.4: Initial portion of Figure 4.4 .....	26
Figure 4.5: Model of the cellular MIMO-OFDM and MIMO MC-CDMA system.....	27
Figure 5.1: BER performance of the MIMO-OFDM system in the two-path channel....	35
Figure 5.2: BER performance of the MIMO-OFDM system in the UMTS defined six-path channel.....	36



Figure 5.3: BER performance of the MIMO MC-CDMA system in the two-path channel with $L = N_u = 256$ i.e., a full-loaded system.....	40
Figure 5.4: BER performance of the MIMO MC-CDMA system in the UMTS defined six-path channel with $L = N_u = 256$ i.e., a full-loaded system.....	41
Figure 5.5: BER performance of the MIMO MC-CDMA system at all four layers in the two-path channel.....	42
Figure 5.6: BER performance of the full-loaded MIMO MC-CDMA system in the two-path channel for different spreading length $L$ .....	43
Figure 5.7: BER performance of the half-loaded MIMO MC-CDMA system in the two-path channel for different spreading length $L$ .....	44
Figure 5.8: BER performance of the MIMO MC-CDMA system for different number of users $N_u$ with fixed spreading length $L = 16$ .....	45
Figure 5.9: BER performance of MIMO-OFDM systems with 1/2-rate convolutional coding and half-loaded MIMO MC-CDMA systems .....	48
Figure 5.10: BER performance of the MIMO-OFDM system in a multi-cell environment with code rate $R = 1/2$ , constraint length $K = 9$ , and $E_b / N_0 = 8\text{dB}$ .....	50
Figure 5.11: BER performance of the half-loaded MIMO MC-CDMA system in a	

multi-cell environment with Walsh codes length  $L=16$  and  $E_b / N_0 = 8\text{dB}$  .....51

Figure 5.12: Simulated distribution of user's average error probability at two tiers'

multi-cell environment..... 53



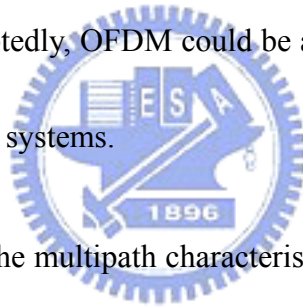
# Chapter 1

## Introduction

Over the past decades, wireless systems continue to strive for ever higher data rates. This goal is particularly challenging for systems that are power, bandwidth, and complexity limited. Multiple-input multiple- output (MIMO) system, which is based on multiple antennas at both the transmitter and receiver, has attracted much attention for its ability to increase channel capacity. It was shown in [1]-[3] that the capacity of MIMO system increases linearly with the minimum of the number of the transmit antennas and the receive antennas. The MIMO system can be exploited to increase the amount of diversity or the spatial degree of freedom of the channel. In this approach, multiple data streams are transmitted simultaneously through different spatial channels, also known as spatial multiplexing. At receive end, many signal process techniques are developed to separate and detect independent information streams. The MIMO technologies can be deployed on various kinds of wireless systems, and their use is now being discussed in several wireless standardization projects.

# 1.1 MIMO-OFDM

Orthogonal frequency division multiplexing (OFDM) has become a popular technique for transmission of signals over wireless channels. The time domain waveforms of the subcarriers are orthogonal, yet the signal spectra corresponding to the different subcarriers overlap in frequency. Hence, the available bandwidth is used very efficiently. OFDM has been adopted in several wireless standards such as digital audio broadcasting (DAB), terrestrial digital video broadcasting (DVB-T), the IEEE 802.11a wireless local area network (WLAN) standard, and IEEE 802.16a. Undoubtedly, OFDM could be a potential air interface candidate for future-generation mobile wireless systems.

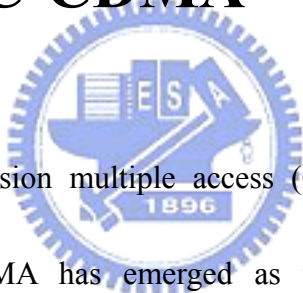


For high data-rate transmission, the multipath characteristic of the environment causes the MIMO channel to be frequency-selective. OFDM can transform such a frequency-selective MIMO channel into a set of parallel frequency-flat MIMO channels, and therefore decrease receiver complexity. The combination of the two powerful techniques, MIMO and OFDM, is very attractive, and has become a most promising broadband wireless access scheme.

In this paper, the vertical BLAST (V-BLAST) architecture proposed in [4] is used. It uses successive interference canceller combined with MMSE or ZF detector to detect signals for different layers. The data which has been detected previously is exploited to reconstruct and cancel layered antenna interference (LAI), and the reliability of the layered interference

cancellation is improved as the interference reduction in the detected signals. However, over the rich scattering environment, the multipath fading channel causes the frequency selective effect. If the signals are transmitted by OFDM systems, serious fading on some subcarriers will degrade the performance [5]. Therefore, a convolutional encoder and a viterbi decoder are added to the system to achieve diversity gains in frequency domain and improve the performance.

## 1.2 MIMO MC-CDMA



In recent years, code division multiple access (CDMA) is one of the most popular transmission techniques. CDMA has emerged as the most important multiple access technology for second- and third-generation (2-3G) wireless systems, exemplified by its popularity in several major mobile cellular standards, such as IS-95, cdma2000, Universal Mobile Telecommunications System (UMTS) terrestrial radio access (UTRA), wideband CDMA (WCDMA), and time-division space/code-division multiple access (TD-SCDMA). Multiple access interference (MAI) is suppressed by spread spectrum techniques, and multipath diversity gain is achieved. However, the data rate throughput is usually sacrificed for getting a large spreading factor.

Multicarrier-code division multiple access (MC-CDMA) can fulfill high data rate multimedia communication and is considered one of the promising techniques for next generation wireless communication systems [5]-[8]. With this technique, a group of data modulated Walsh codes is transmitted over multiple subcarriers to achieve high data rate throughput. However, in a mobile radio environment, a multipath channel will introduce severe multipath interference (MPI) and destroy the orthogonality among the Walsh codes. As a result, the multipath phenomenon significantly degrades the data rate throughput of a multi-code system. Therefore, [9]-[12] suggested a multistage multipath interference cancellation (MPIC) technique to eliminate the MPI in the received signal and achieve higher data rate throughput.



## 1.3 About The Thesis

This thesis is organized as follows. The MIMO-OFDM and MIMO MC-CDMA system models are described in Chapter 2. The details of the detection methods for the two systems are included in Chapter 3. The model for the different propagation impairments affecting the cellular environments is described in Chapter 4. The performance of the MIMO-OFDM and MIMO MC-CDMA systems are evaluated and compared through computer simulations in Chapter 5. Finally, some conclusions are drawn in the last chapter.

# Chapter 2

## System Model

In this chapter, the MIMO-OFDM and MIMO MC-CDMA system models are presented.

They both apply  $M$  antennas to transmit different data, so spectral efficiency becomes  $M$  times.

The details of system model are described and illustrated as follows.

### 2.1 MIMO-OFDM



Figure 2.1 shows a transmitter block diagram of the MIMO-OFDM system with  $M$  transmit antennas. The information source output is first encoded by a convolutional channel-coder, and interleaved by the interleaver  $\Pi$ . The encoded bits are then mapped into QPSK symbols and serial-to parallel (S/P) converted into  $M$  parallel data substreams. Each data substream is fed into an OFDM modulator, which induces  $N$ -point inverse discrete Fourier transform (IFFT) block followed by a parallel to serial (P/S) block and guard interval insertion (GI). The resultant  $M$  signals are transmitted simultaneously.

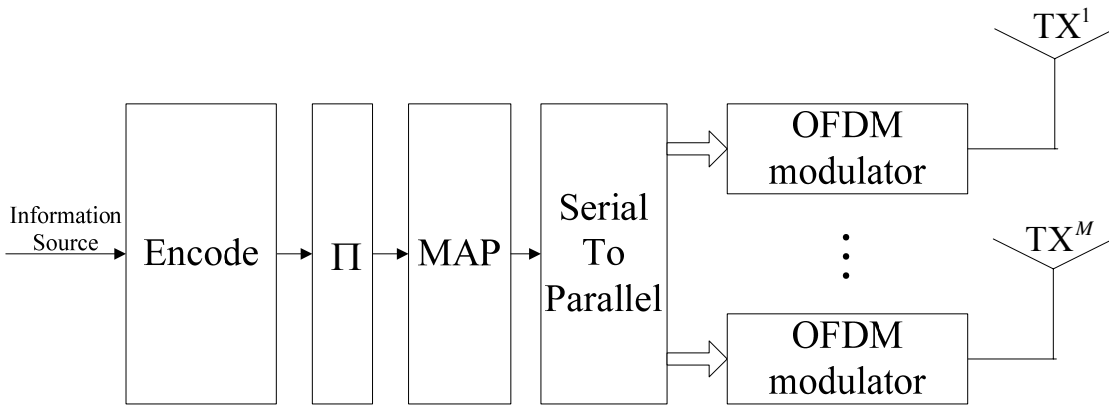


Figure 2.1: The transmitter block diagram of the MIMO-OFDM system

## 2.2 MIMO MC-CDMA

Figure 2.2 shows a transmitter block diagram of the MIMO MC-CDMA system with  $M$  transmit antennas. The information source output is first S/P converted into  $M$  parallel data streams  $d^m$ , for  $1 \leq m \leq M$ .

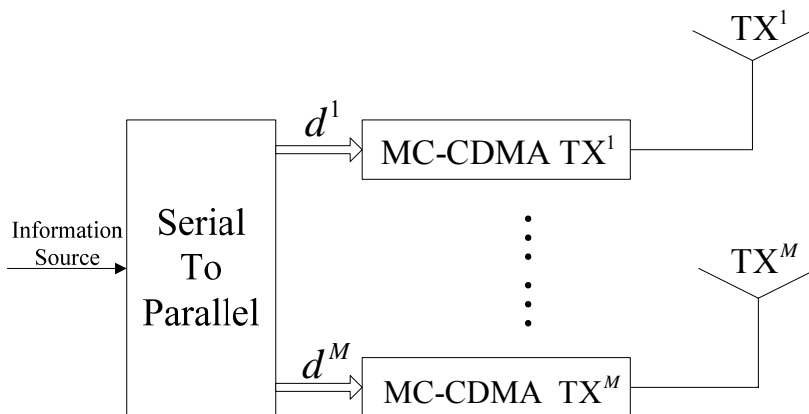


Figure 2.2: The transmitter block diagram of the MIMO MC-CDMA system

Each data stream is then processed by an MC-CDMA transmission scheme and sent to the



corresponding transmit antenna. The MC-CDMA transmission scheme for the  $m$ th transmit antenna is shown in Figure 2.3. After S/P conversion, the  $m$ th data stream  $d^m$  is first mapped into QPSK symbols and multiplexed to  $N_d = N/L$  parallel data substreams  $\mathbf{b}_n^m$ , for  $1 \leq n \leq N_d$  where  $L$  is the length of a Walsh code. Each Walsh code  $\mathbf{c}_k$  is defined as a vector  $\mathbf{c}_k = [c_{k,1}, c_{k,2}, \dots, c_{k,L}]^T$  where  $c_{k,l} \in \{1, -1\}$  denotes the  $l$ th chip of the  $k$ th Walsh code, for  $1 \leq l \leq L$ . Each data substream  $\mathbf{b}_n^m = [b_{n,1}^m, b_{n,2}^m, \dots, b_{n,N_u}^m]^T$  is then spread by a group of Walsh codes,  $\mathbf{c}_k$ , for  $k = 1, \dots, N_u$ . The data modulated Walsh codes are summed up and the sum can be expressed as  $\mathbf{s}_n^m = \mathbf{C}_L \mathbf{b}_n^m = \sum_{l=1}^{N_u} b_{n,l}^m \mathbf{c}_l$ , for  $1 \leq n \leq N_d$ . After S/P converted, the data symbols are interleaved by the random interleaver  $\Pi^m$  to maximize the diversity gain and avoid coherent IAI at the receiver side. The system load is  $N_u/L$  and can be set to a value from 1 to  $1/L$ . As a result, the transmitted signal in frequency domain from the  $m$ th transmit antenna can be written as

$$\begin{aligned} \mathbf{x}^m &= [x_1^m, x_2^m, \dots, x_N^m]^T = \Pi^m \{ \mathbf{s}^m \} \\ &= \Pi^m \left\{ \left[ (\mathbf{s}_1^m)^T, (\mathbf{s}_2^m)^T, \dots, (\mathbf{s}_{N_d}^m)^T \right]^T \right\} \end{aligned} \quad (2.1)$$

After interleaving, the signals are fed into an OFDM modulator and the resultant  $M$  signals are transmitted simultaneously.

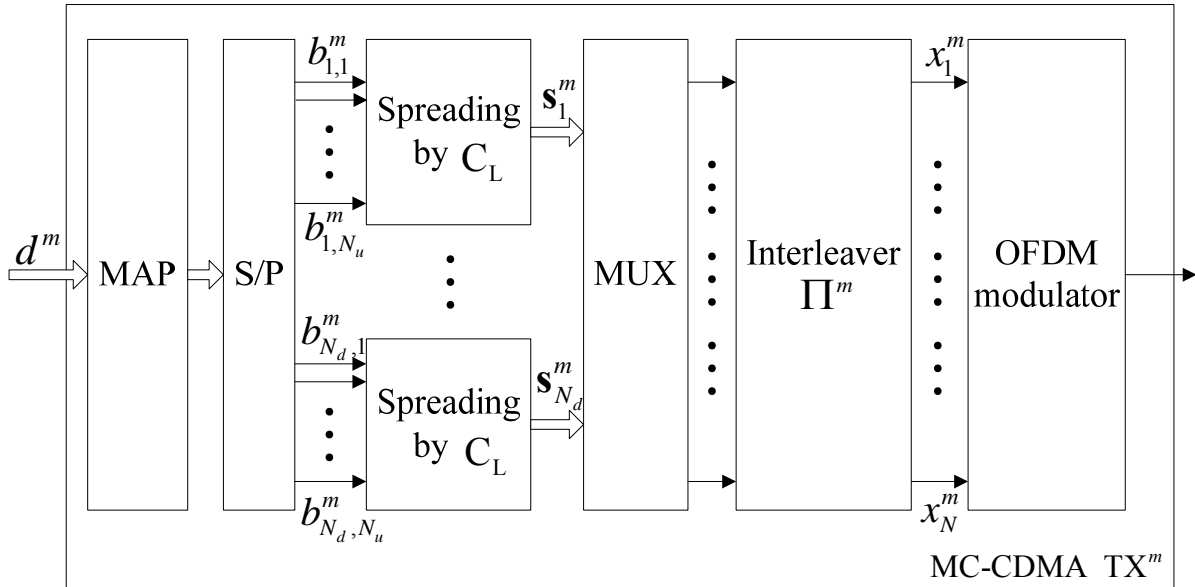


Figure 2.3: The MC-CDMA transmit scheme at the  $m$ th transmit antenna



For simplification, we assume that the synchronization and channel estimation at the receivers are perfect and the maximum multipath delay spread is fewer than  $T_g$ , the time duration of GI. So receivers can obtain the accurate channel information and be ISI-free.

# Chapter 3

## Detection Methods for MIMO-OFDM and MIMO MC-CDMA Systems

In both MIMO systems, each transmitter is used to transmit different data stream that induces the inter antenna interference (IAI). The received signals for MIMO-OFDM systems and MIMO MC-CDMA systems all contain IAI. The data stream for individual transmitter must be detected from signals at  $J$  receivers. Each layer is considered in turn to be the desired signal, and the remainder is treated as interference (Successive Interference Cancellation, SIC). The signal processing chain related to each individual data substream from a transmit antenna is referred to as a layer. The signal processing of the  $Q$ th layer is called the  $Q$ th layered detection. For MIMO-OFDM systems, the ordering of layered detections gives effect to the performance of the SIC detector. On the other hand, for MIMO MC-CDMA systems the iterative multi-layered detection method is not sensitive to the order of the layer processing. Therefore without loss of generality, the layered detection is started with the first layer and is done in a round robin fashion. In the following, we first describe the V-BLAST detection for MIMO-OFDM systems in subsection 3.1. In subsection 3.2, we describe the detection methods for MIMO MC-CDMA systems, which contain the layered antenna interference

cancellation (LAIC) concept, the adaptive MMSE equalizer, and the MPIC method. The iterative multi-layered detection method is summarized at the end of the section.

### 3.1 V-BLAST Detection Methods for MIMO-OFDM Systems

The received signal vector in frequency domain for the  $i$ th subcarrier and all  $J$  receive antennas  $\mathbf{r}_i$  can be expressed as

$$\mathbf{r}_i = \mathbf{H}_i \mathbf{x}_i + \mathbf{n}_i \tag{3.1}$$

where  $\mathbf{H}_i$ ,  $\mathbf{x}_i$ , and  $\mathbf{n}_i$  are the  $J \times M$  channel matrix with element  $h_i^{j,m}$  representing the channel frequency response between the  $m$ th transmit antenna and the  $j$ th receive antenna at the  $i$ th subcarrier, the  $M \times 1$  vector for the transmitted signal form all  $M$  transmit antennas, and the  $J \times 1$  noise vector at  $J$  receive antennas.

In [4], a V-BLAST architecture is proposed which can be used for MIMO-OFDM systems. Signals for different layers are detected by the successive interference canceller combined with MMSE criterion. As mentioned in [13], when symbol cancellation is used, the system performance is affected by the order in which the components are detected. Because the operations are the same for all subcarriers, the subcarrier index  $i$  is omitted below. The matched signal is  $\mathbf{z} \triangleq \mathbf{H}^H \mathbf{r} = \mathbf{H}^H \mathbf{H} \mathbf{x} + \mathbf{H}^H \mathbf{n}$ . The full MMSE V-BLAST detection algorithm

(see Appendix A) can now be described compactly as a recursive procedure, including determination of the optimal ordering, as follows:

*Initialization*

$$i \leftarrow 1 \quad (3.2)$$

$$\mathbf{G}_1 = \mathbf{H}^+ \triangleq (\mathbf{H}^H \mathbf{H} \mathbf{H}^H \mathbf{H} + \sigma_n^2 \mathbf{H}^H \mathbf{H})^{-1} \mathbf{H}^H \mathbf{H} \quad (3.3)$$

$$k_1 = \arg \min_m \|(\mathbf{G}_1)_m\|^2 \quad (3.4)$$

*Recursion*

$$\mathbf{w}_{k_i} = (\mathbf{G}_i)_{k_i} \quad (3.5)$$

$$y_{k_i} = \mathbf{w}_{k_i}^T \mathbf{z}_i \quad (3.6)$$

$$\hat{x}_{k_i} = \text{HARD}(y_{k_i}) \quad (3.7)$$

$$\mathbf{r}_{i+1} = \mathbf{r}_i - \hat{x}_{k_i} (\mathbf{H})_{k_i} \quad (3.8)$$

$$\mathbf{H}_{i+1} = \mathbf{H}_{\bar{k}_i} \quad (\text{zeroing columns } k_1, k_2, \dots, k_i \text{ of } \mathbf{H}) \quad (3.9)$$

$$\mathbf{G}_{i+1} = \mathbf{H}_{i+1}^+ \quad (3.10)$$

$$\mathbf{z}_{i+1} = \mathbf{H}_{i+1}^H \mathbf{r}_{i+1} \quad (3.11)$$

$$k_{i+1} = \arg \min_{m \notin \{k_1, k_2, \dots, k_i\}} \|(\mathbf{G}_{i+1})_m\|^2 \quad (3.12)$$

$$i \leftarrow i + 1 \quad (3.13)$$

It should be noticed that the V-BLAST architecture described above is a modified version of [4]. We have added a matched filter at the receiver to improve the system performance. By

rewriting Eq. (3.3) as  $\mathbf{G}_1 = \mathbf{H}^+ \triangleq \text{inv}(\mathbf{H}^H \mathbf{H} + \sigma_n^2 \mathbf{I}_M) \mathbf{H}^H$  and removing the matched filter, we can obtain the original V-BLAST architecture proposed in [4].

After the V-BLAST detection is done, the decision results are deinterleaved and decoded by a Viterbi decoder, as shown in Figure 3.1.

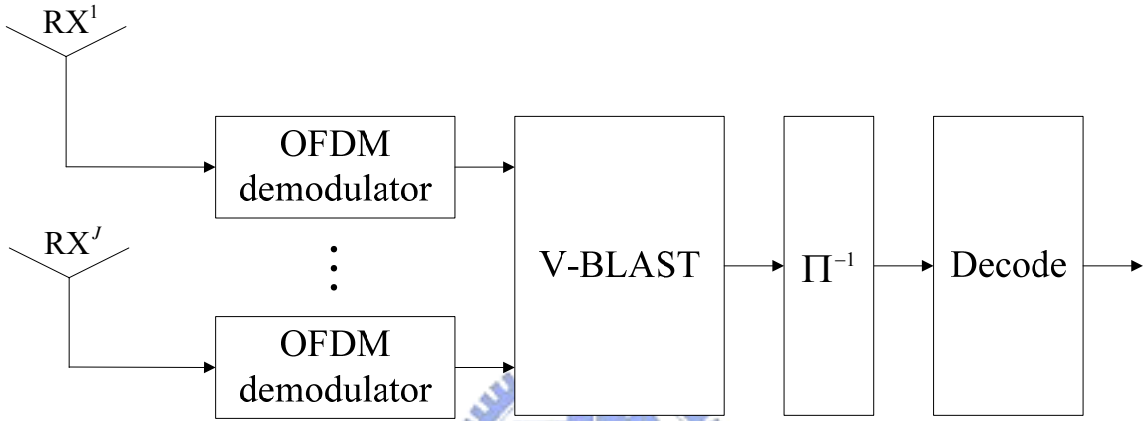


Figure 3.1: The receiver block diagram of the MIMO-OFDM system

## 3.2 Iterative Multi-layered Detection Methods for MIMO MC-CDMA Systems

The notation for MIMO-CDMA systems is slightly different from that for MIMO-OFDM systems. The received signal in frequency domain at the  $j$ th receive antenna can be written as:

$$\mathbf{r}^j = \sum_{m=1}^M \mathbf{H}^{j,m} \mathbf{x}^m + \mathbf{n}^j \quad (3.14)$$

Where  $\mathbf{r}^j = [r_1^j, r_2^j, \dots, r_N^j]^T$ ,  $\mathbf{H}^{j,m} = \text{diag}\{h_1^{j,m}, h_2^{j,m}, \dots, h_N^{j,m}\}$ , and  $\mathbf{n}^j = [n_1^j, n_2^j, \dots, n_N^j]^T$  are

the received signal vector, channel frequency response matrix from the  $m$ th transmit antenna to the  $j$ th receive antenna ( $N \times N$  diagonal matrix), and noise vector at the  $j$ th receive antenna, respectively. The matrix  $\mathbf{H}^{j,m}$  can be expressed as  $\mathbf{H}^{j,m} = \sum_{p=1}^P \mathbf{H}_p^{j,m}$  in more details, where  $P$  is the total number of paths.  $\mathbf{H}_p^{j,m}$  is the channel frequency response of the  $p$ th path, which is diagonal with each element  $\alpha_p^{j,m} \exp\{j2\pi(i-1)\tau_p^{j,m}/N\}$ , for  $1 \leq i \leq N$ , where  $\alpha_p^{j,m}$  and  $\tau_p^{j,m}$  are the complex fading gain and the excess delay of the  $p$ th path, respectively. The  $N$  elements of  $\mathbf{n}^j$  are modeled as independent complex Gaussian random variables with zero mean and variance  $\sigma_n^2$ .

### 3.2.1 Layered Antenna Interference Cancellation and Adaptive MMSE Equalization

From Eq. (3.14), it is apparent that the orthogonality of Walsh codes will be destroyed when the channel is frequency selective. Under such circumstances, the system encounters not only severe IAI but also severe MPI which together degrade the system performance.

At the  $Q$ th layered detection, the hard decision results  $\hat{\mathbf{x}}^m$  of the previous  $(Q-1)$  layers, for  $1 \leq m \leq (Q-1)$  can be used to generate the IAI replicas. After subtracted from the received signal  $\mathbf{r}^j$  of the  $j$ th receive antenna, the resulting signal is

$$\tilde{\mathbf{r}}^{j,Q} = \mathbf{r}^j - \sum_{m=1}^{Q-1} \mathbf{H}^{j,m} \hat{\mathbf{x}}^m \quad (3.15)$$

Then, we apply a simple frequency domain adaptive MMSE equalizer  $\mathbf{G}^{j,Q}$  without matrix inversion to the signal  $\tilde{\mathbf{r}}^{j,Q}$  [14]. It can be formulated by  $\mathbf{G}^{j,Q} = \text{diag}\{g_1^{j,Q}, g_2^{j,Q}, \dots, g_N^{j,Q}\}$ .

Assume that the hard decision results of the previous layers are all correct, i.e. the IAI is perfectly removed. Besides, due to the use of the interleaver at the transmitter side, we can treat the unprocessed IAI as noise. Therefore, the coefficients of the adaptive MMSE equalizer can be expressed as

$$g_i^{j,Q} = \frac{(h_i^{j,Q})^*}{|h_i^{j,Q}|^2 + \frac{\sigma_i^2}{2L}} \quad (3.16)$$

where  $\sigma_i^2 = \sigma_n^2 + 2N_u \sum_{m=Q+1}^M |h_i^{j,m}|^2$ , for  $1 \leq i \leq N$ . Hence, after equalization and deinterleaving,

the signal becomes

$$\boldsymbol{\gamma}^{j,Q} = (\boldsymbol{\Pi}^Q)^{-1} \{ \mathbf{G}^{j,Q} \tilde{\mathbf{r}}^{j,Q} \} \quad (3.17)$$

In the case of  $N_d > 1$ , the despreading process does not require the whole  $N$  elements of  $\boldsymbol{\gamma}^{j,Q}$

but only a segment with length  $L$ . Write  $\boldsymbol{\gamma}^{j,Q}$  as

$$\boldsymbol{\gamma}^{j,Q} = \left[ \underbrace{\gamma_1^{j,Q}, \dots, \gamma_L^{j,Q}}_{\boldsymbol{\gamma}_1^{j,Q}}, \underbrace{\gamma_{L+1}^{j,Q}, \dots, \gamma_{2L}^{j,Q}}_{\boldsymbol{\gamma}_2^{j,Q}}, \dots, \underbrace{\gamma_{N-L+1}^{j,Q}, \dots, \gamma_N^{j,Q}}_{\boldsymbol{\gamma}_{N_d}^{j,Q}} \right]^T \quad (3.18)$$

The  $u$ th code channel output  $z_u^Q$  after despreading and receiver diversity combining is

$$z_u^Q = \sum_{j=1}^J \mathbf{c}_\mu^T \cdot \boldsymbol{\gamma}_\mu^{j,Q}, \text{ where } \mu = u \bmod N_u, \mu' = \lceil u/N_u \rceil.$$

### 3.2.2 Multipath Interference Cancellation



After first iteration, hard decision results of all layers are available. At the  $j$ th receive antenna and the  $Q$ th layered detection, a signal  $\bar{\mathbf{r}}^{j,Q}$  can be obtained by subtracting the IAI from the received signal  $\mathbf{r}^j$ , that is,

$$\bar{\mathbf{r}}^{j,Q} = \mathbf{r}^j - \sum_{m=1, m \neq Q}^M \mathbf{H}^{j,m} \hat{\mathbf{x}}^m \quad (3.19)$$

With the hard decision results of the  $Q$ th data substream, the MPIC method can be used to suppress the MPI and to achieve multipath diversity gains [9]-[12]. The details operations of the MPIC method are summarized as follows. First, the MPI replicas of all interfering signal paths can be generated and subtracted from the signal  $\bar{\mathbf{r}}^{j,Q}$  to extract the signal from each path  $\bar{\mathbf{r}}_v^{j,Q}$

$$\bar{\mathbf{r}}_v^{j,Q} = \bar{\mathbf{r}}^{j,Q} - \sum_{p=1, p \neq v}^P \mathbf{H}_p^{j,Q} \hat{\mathbf{x}}^p \quad (3.20)$$

, for  $1 \leq v \leq P$ . After RAKE combining and deinterleaving, the signal becomes

$$\boldsymbol{\chi}^{j,Q} = (\Pi^Q)^{-1} \left\{ \sum_{v=1}^P (\mathbf{H}_v^{j,Q})^H \bar{\mathbf{r}}_v^{j,Q} \right\} \quad (3.21)$$

In the case of  $N_d > 1$ , the despreading process does not require the whole  $N$  elements of  $\boldsymbol{\chi}^{j,Q}$  but only a segment with length  $L$ . Write  $\boldsymbol{\chi}^{j,Q}$  as

$$\boldsymbol{\chi}^{j,Q} = \left[ \underbrace{\chi_1^{j,Q}, \dots, \chi_L^{j,Q}}_{\chi_1^{j,Q}}, \underbrace{\chi_{L+1}^{j,Q}, \dots, \chi_{2L}^{j,Q}}_{\chi_2^{j,Q}}, \dots, \underbrace{\chi_{N-L+1}^{j,Q}, \dots, \chi_N^{j,Q}}_{\chi_{N_d}^{j,Q}} \right]^T \quad (3.22)$$

The  $u$ th code channel output  $\bar{z}_u^Q$  after despreading and receiver diversity combining is  $\bar{z}_u^Q = \sum_{j=1}^J \mathbf{c}_\mu^T \cdot \boldsymbol{\chi}_\mu^{j,Q}$ . We can then detect the  $u$ th data symbol by determining whether the real part (or the imaginary part) of  $\bar{z}_u^Q$  is greater or lesser than zero by hard decision.

### 3.2.3 Iterative Multi-layered Detection

The iterative multi-layered detection method is summarized as follows. Figure 3.1 shows the first iteration of our multi-layered detection method. The signal is processed according to the LAIC concept and the adaptive MMSE equalization method as described in subsection 3.2.1. Note that at the first layered detection, the received signals are passed only through the adaptive MMSE equalizer to obtain the hard decision results for the first data substream.

Figure 3.2 shows the second and subsequent iterations of the iterative multi-layered detection method. For illustration purpose, we focus on the  $Q$ th layered detection for the  $j$ th receive antenna for the second iteration. Because we have the hard decision results of all the data substreams, the LAIC eliminates all the other data substreams (excluding the  $Q$ th data substream) according to Eq. (3.19) to obtain the signal  $\bar{\mathbf{r}}^{j,Q}$ . Afterward, we use the adaptive MMSE equalizer with coefficients of  $g_i^{j,Q} = (h_i^{j,Q})^* / (|h_i^{j,Q}|^2 + \sigma_n^2/2L)$ , for  $1 \leq i \leq N$ , to equalize the signal  $\bar{\mathbf{r}}^{j,Q}$  and obtain more reliable decision results of the  $Q$ th data substream. At this point, the MPIC method mentioned in subsection 3.2.2 is executed according to Eq. (3.20) and Eq. (3.21) to obtain the decision results of the  $Q$ th data substream. In general, the decision result is much more accurate by fully exploiting the gains from both the spatial diversity and the multipath diversity. The process can be repeated in several iterations until

reliable data estimates of all the data substreams are obtained. Note that for the last few iterations, because the adaptive MMSE equalizer can not have further improvement in BER performance, the MPIC can be executed alone without the help from the adaptive MMSE equalizer to accelerate the convergence process.



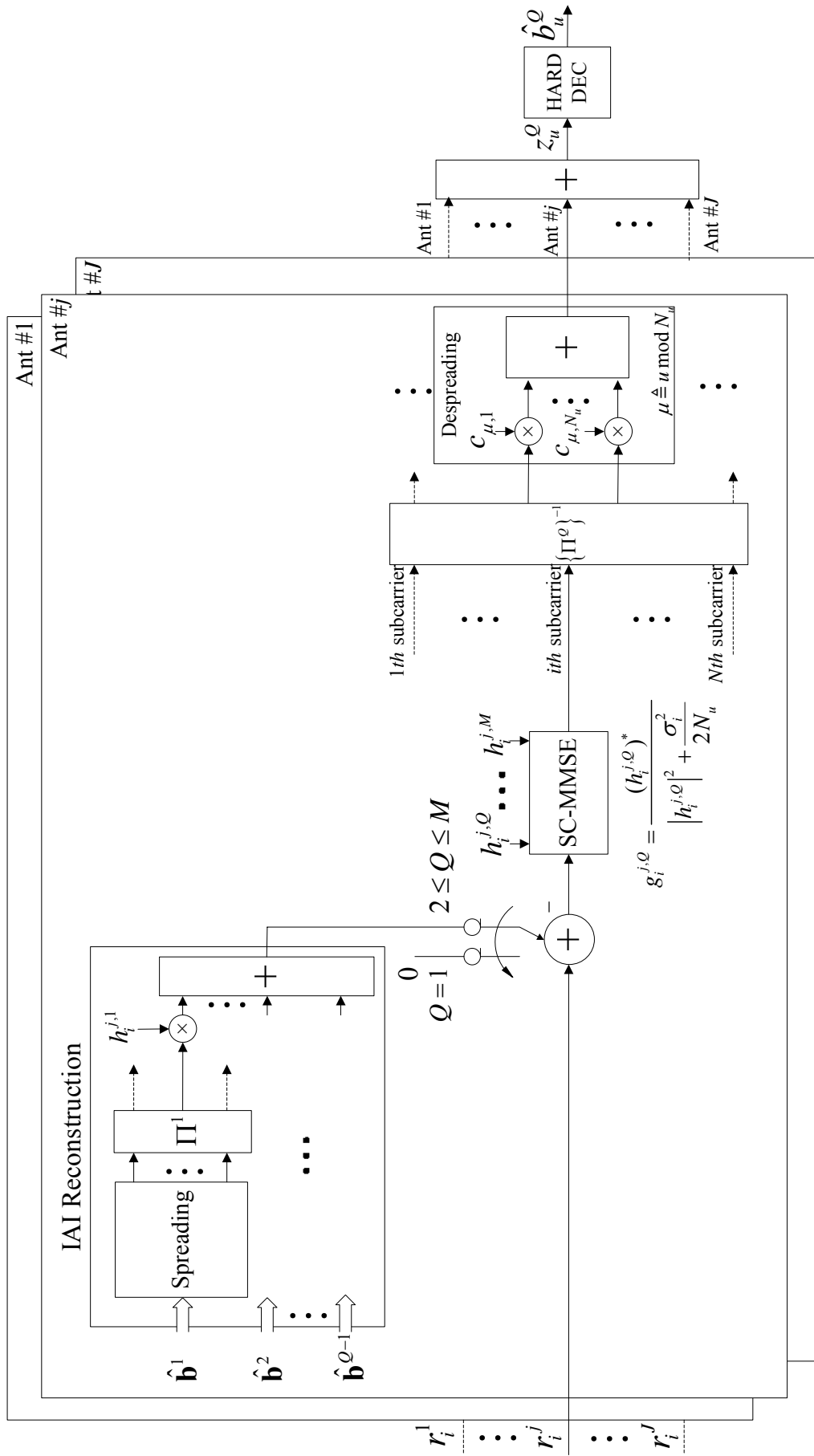


Figure 3.1: The first iteration of the multi-layered detection method

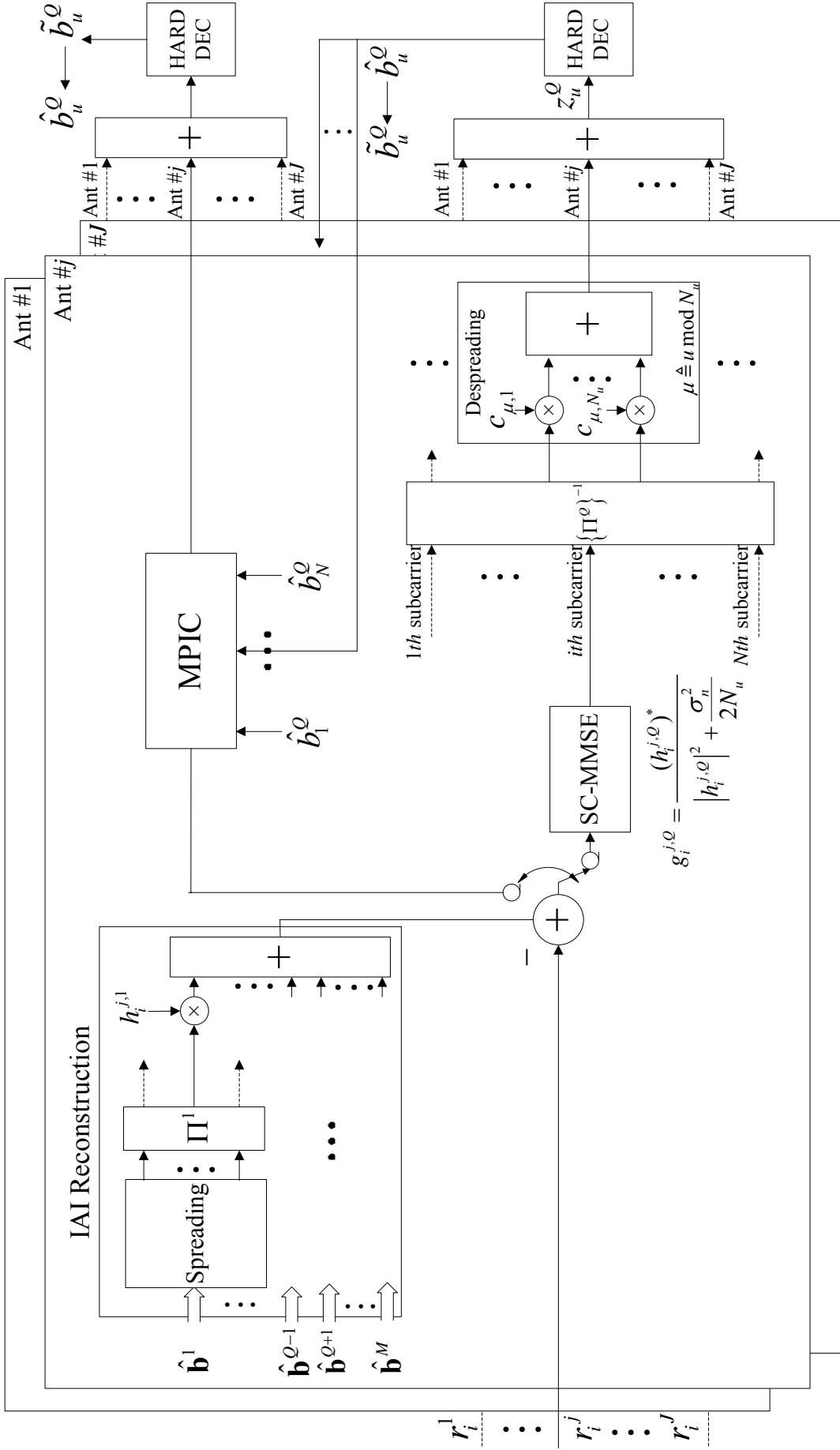
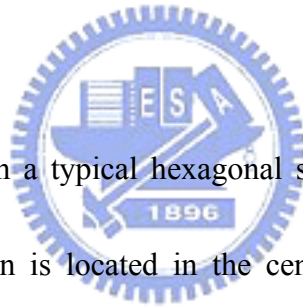


Figure 3.2: The second and latter iterations of the multi-layered detection method

# Chapter 4

## Multi-cell Environment

Here we present a cellular network. Furthermore, a propagation model for the path loss is introduced and described in detail.



The cellular network is based on a typical hexagonal structure where all cell sizes are assumed to be equal. A base station is located in the center of each cell. The multi-cell environment consists of  $(I + 1)$  base stations where the center base station, denoted as  $BS_{(0)}$ , is surrounded by interfering base stations, denoted as  $BS_{(i)}$ , for  $1 \leq i \leq I$ .

### 4.1 Propagation Loss Model

The propagation attenuation is generally modeled as the product of the  $\rho$ th power of distance and a log-normal component representing shadowing loss [15]. Shadow variations

are caused by large terrain features between the base station and the mobile station such as buildings and hills. These represent slowly varying variations even for users in motion and apply to both downlink and uplink. Thus for a user at a distance  $d$  from a base station, the received signal energy  $E_r$  can be modeled as

$$E_r = E_t \times d^{-\rho} \times 10^{\eta/10} \quad (4.1)$$

where  $E_t$  is the transmitted signal energy. Furthermore, the shadowing factor  $\eta$  is a normally distributed random variable with zero mean and standard deviation  $\sigma_p$  and is given in dB. In [16], the standard deviation  $\sigma_p$  and the distance decay factor  $\rho$  are set to 8 dB and 4, respectively, as suggested by experimental data. These values are used throughout this paper unless further mentioned.



## 4.2 Distributions of Signal-to-Noise Ratio

The following is a list of assumptions from which we depart to establish a multi-cell environment.

- 1). Our system performance is limited by interference coming from users within the same frequency band.

- 2). The information data signaling rate is low enough such that ISI can be neglected.
- 3). Uplink transmission and downlink transmission have to be separated.
- 4). Each base station transmits at the same power level in its downlink channels.
- 5). Every mobile station transmits at a power level such that its home base always receives at the same power level, i.e., power control is executed in uplink transmissions.
- 6). The uplink and downlink channel are reciprocal from propagation loss point of view.
- 7). A mobile station always chooses its home base station to be the one provides the largest received signal power level.



Here we use computer simulation to calculate SIR [17]. The propagation loss model is used as described in subsection 4.1.

$$\text{SIR} = \frac{d_0^{-\rho} \times 10^{\eta_0/10}}{\sum_{i=1}^I d_i^{-\rho} \times 10^{\eta_i/10}} \quad (4.2)$$

where  $d_i$  is the distance between the mobile station and  $\text{BS}_{(i)}$ , and  $\eta_i$  is a normally independent distributed random variable with zero mean and standard deviation  $\sigma_p$  for all  $i$ .

Figure 4.2 shows the simulated cumulative distribution of downlink SIR when the whole system consists of 2~61 cells. In the simulation, a candidate mobile station is randomly located within the central cell and the received signal power level from each base station is calculated according to the mentioned propagation loss model. The base associated with the



largest received signal power level is regarded as the home base and the signals from all the other bases are regarded as interference. In order to examine the distribution curves more closely, we expand the initial portion of curves in Figure 4.1 in Figure 4.2. From Figure 4.2 we observe that downlink SIR is better than -5.0, -4.5, and -3.4 dB for more than 99 percent of the simulated cases when the number of tiers is 4, 2, and 1, respectively.

The simulation of uplink SIR is trickier than the downlink case. Take the 4 tiers case as an example, we first generate a table of size  $60 \times 10000$  from the downlink simulation. During each run of downlink simulation we found a home base for a candidate mobile randomly located in the central cell. Each row of the table was then generated such that it consists of normalized interference power received at the mobile from 60 bases around the home base. By normalization we mean the dividing of the received power from each surrounding base by the power received from the home base. As a result, each item in the table is less than or equal to one. The table can be interpreted as a sample space of normalized interference from each of the 60 surrounding bases to a user associated with the home base. Due to power level reciprocity the table can also be interpreted as a sample space of normalized interference from a user associated with the home base to its 60 surrounding bases when uplink power control is in effect. Figure 4.3 shows the simulated cumulative distribution of uplink SIR under the assumption that a candidate home base station is located at the central cell and each base station has a mobile station in communication with it. The wanted signal comes from the

mobile associated with the central home base and the interference comes from all other mobiles associated with surrounding bases. Figure 4.4 expands the initial portion of the distribution curves in Figure 4.3. From Figure 4.4 we see that uplink SIR is better than -3.1, -2.9, and -2.2 dB for more than 99% of the simulated cases when the number of tiers is 4, 2, and 1, respectively. The simulation results indicate that uplink SIR is better than the downlink case.



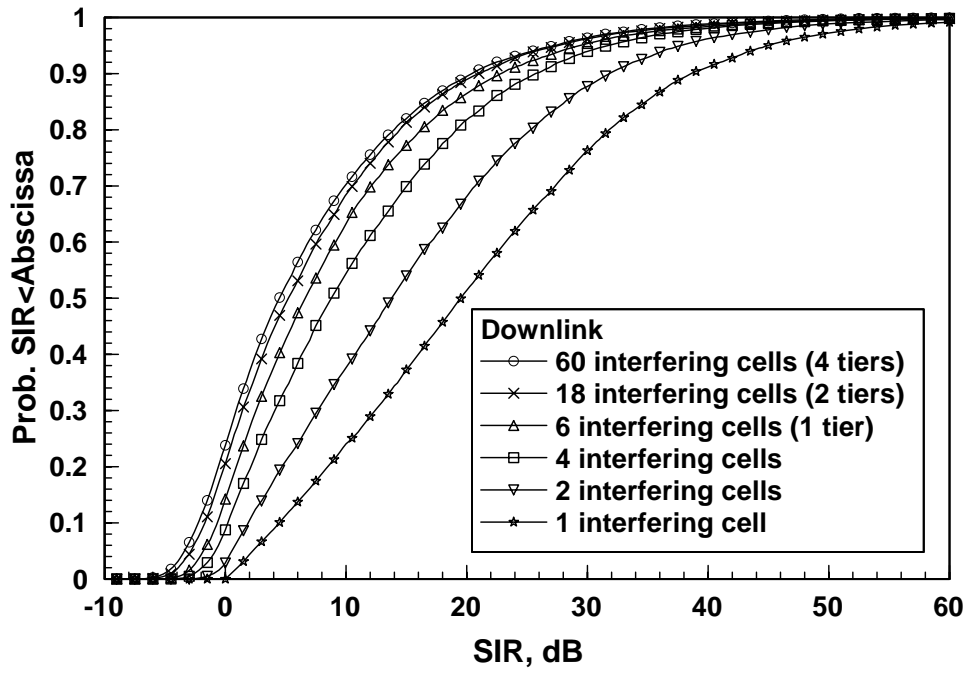


Figure 4.1: Simulated distribution of Downlink SIR

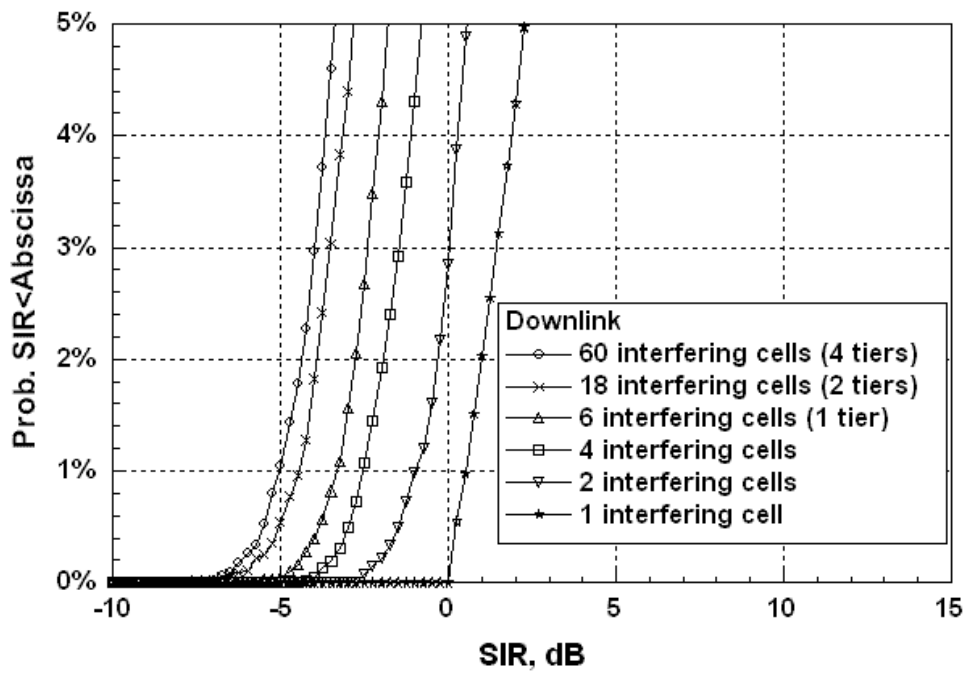


Figure 4.2: Initial portion of Figure 4.2

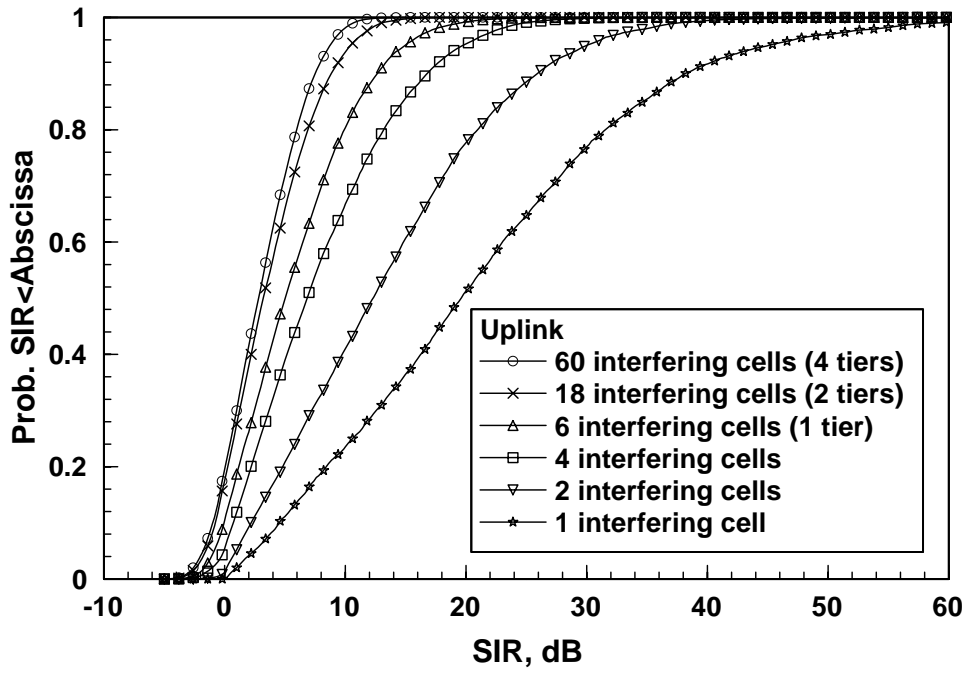


Figure 4.3: Simulated distribution of Uplink SIR

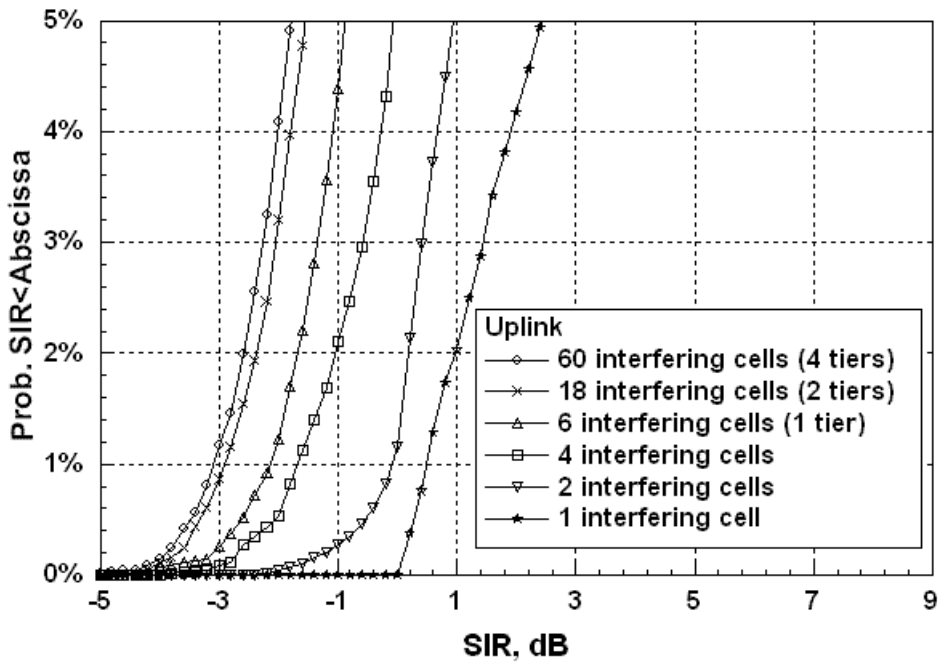


Figure 4.4: Initial portion of Figure 4.4

## 4.3 Cellular Interference Modeling

The cellular interference can be modeled as depicted in Figure 4.5. We assume the synchronization between the base station and the mobile station is perfect.

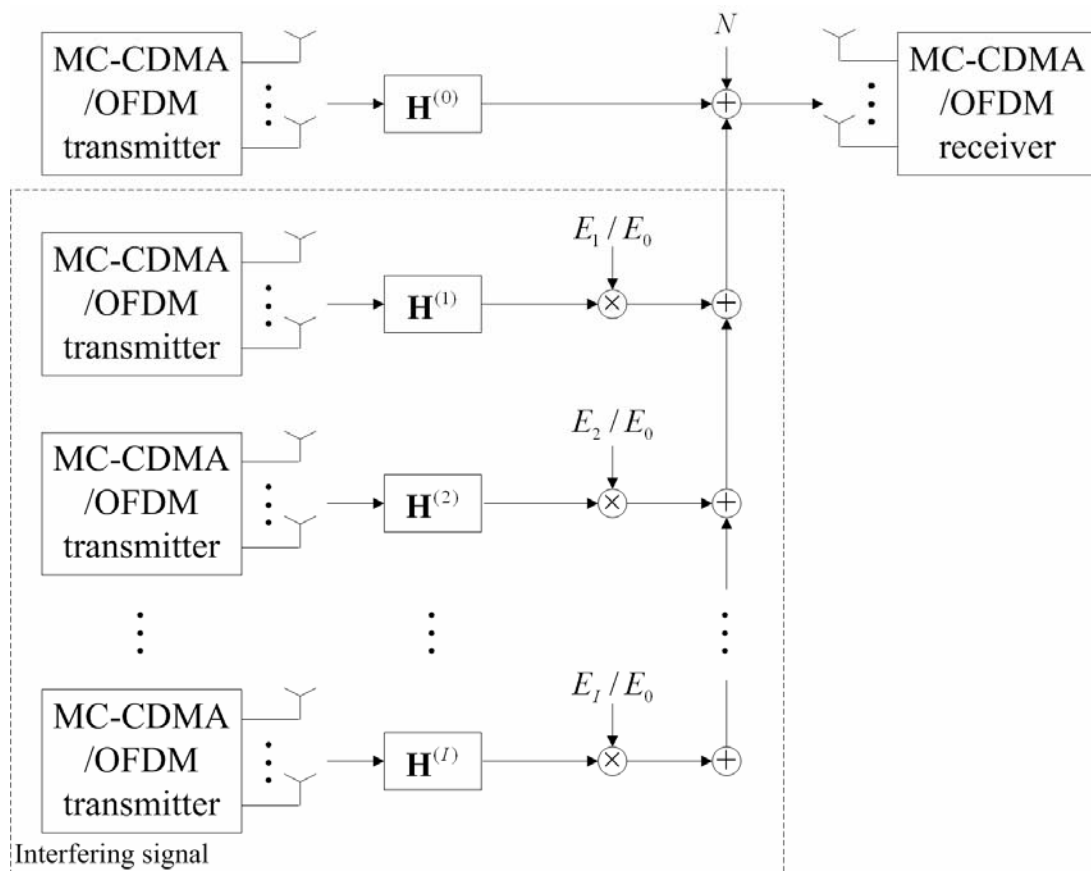


Figure 4.5: Model of the cellular MIMO-OFDM and MIMO MC-CDMA system

By including the interfering base stations the received signal in frequency domain becomes (for similarity, we omit the subcarrier index)

$$\mathbf{y} = E_0 \mathbf{H}^{(0)} \mathbf{x}^{(0)} + \sum_{i=1}^I E_i \mathbf{H}^{(i)} \mathbf{x}^{(i)} + \mathbf{n} \quad (4.3)$$

where  $\mathbf{H}^{(i)}$ ,  $\mathbf{x}^{(i)}$ ,  $\mathbf{y}$ , and  $\mathbf{n}$  are the  $J \times M$  MIMO channel matrix between the  $i$ th transmitter and the receiver,  $M \times 1$  transmitted signal vector from the  $i$ th transmitter,  $J \times 1$  received signal vector, and  $J \times 1$  noise vector, respectively. The signal energy of the  $i$ th transmitter  $E_i$  can be modeled according to Eq. (4.1).

### 4.3.1 Gaussian Approximation



For system level simulations, the simulation of all interfering signal paths is very complex. Thus, a simplification of the interference model is done by assuming the entire interference as Gaussian noise [18]. Hereby, the noise variance has to be scaled appropriately. By Gaussian approximation, Eq. (4.2) can be rewritten as

$$\mathbf{y} \approx E_0 \mathbf{H}_{(0)} \mathbf{x}_{(0)} + \mathbf{n}_I + \mathbf{n} \quad (4.3)$$

If all path gains have unit mean, the variance of the Gaussian approximated interference  $\mathbf{n}_I$  will be  $M \sum_{i=1}^I E_i$ . With the Gaussian approximation, no information about the interfering

signal is needed, except for their average signal strength. Thus, a multi-cell environment can be implemented very efficiently. The Gaussian approximation is suitable because  $\mathbf{H}_{(i)}$  is Gaussian.  $\mathbf{x}_{(i)}$  is not Gaussian since it is randomly taken from a finite set  $\{\pm 1 \pm j\}$ .



# Chapter 5

## Simulation Results

### 5.1 Simulation Environments

We verify and compare the performance of the MIMO-OFDM and MIMO MC-CDMA systems by computer simulations. A frequency selective channel is modeled and the equivalent baseband impulse response of the multipath channel between the  $m$ th transmit and the  $j$ th receive antenna is represented by

$$h^{j,m}(t) = \sum_{p=1}^P a_p^{j,m} \delta(t - \tau_p^{j,m}) \quad (5.1)$$

for  $1 \leq m \leq M$ ,  $1 \leq j \leq J$ , where  $P$  is the number of resolvable paths;  $\tau_p^{j,m}$  is the excess delay of the  $p$ th path from the  $m$ th transmit antenna and the  $j$ th receive antenna;  $a_p^{j,m}$  is the complex fading gain of the  $p$ th path, which is complex Gaussian random variable, and  $\delta(t)$  denotes a delta function. The fading patterns of each temporally resolvable path from each transmit antenna to the receive side are generated independently. It is assumed that the channel is stationary over each transmission. Two channel models are selected for our simulations. One is a two-path channel with relative path power profiles: 0, 0 (dB). The other



is a Universal Mobile Telecommunication System (UMTS) defined six-path channel with relative path power profiles: -2.5, 0, -12.8, -10, -25.2, -16 (dB) [19].

Table 5.1 shows the simulation parameters commonly used for both MIMO-OFDM and MIMO MC-CDMA systems. The entire simulations are conducted in the equivalent baseband. We assume symbol synchronization, carrier synchronization, and channel state information are perfectly estimated. The noise and interference power are also assumed to be known at the receiver end. The excess delay of the paths is uniformly distributed between  $0\mu\text{s}$  and  $12.3\mu\text{s}$ . In the multi-cell environment, all interfering cells have the same parameters as the desired cell.

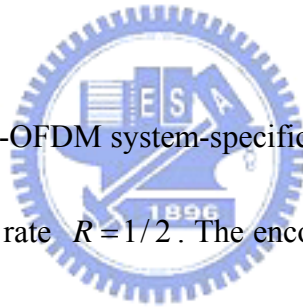


Table 5.2 shows the MIMO-OFDM system-specific simulation parameters. We choose the convolutional codes with fixed rate  $R=1/2$ . The encoders are listed in Table 5.3. Each code is chosen to have maximum free distance [20].

Table 5.4 shows the MIMO MC-CDMA system-specific simulation parameters. The number of Walsh codes is equivalent to the length of each Walsh code. Therefore, when there are  $N_u$  active users, the system load will be  $N_u/L$  which can be set to a value ranging from 1 to  $1/L$ .

# transmit antenna	$M$	4
# receive antenna	$J$	4
Modulation		QPSK
Carrier frequency	$f_c$	2GHz
Total Bandwidth	$B_w$	5.12MHz
# subcarriers	$N$	256
Guard interval	$T_g$	12.5 $\mu$ s
# resolvable paths	$P$	2 or 6

Table 5.1: Simulation parameters common for both MIMO-OFDM and MIMO MC-CDMA systems

Channel coding		Convolutional code
Channel coding rate	$R$	1/2

Table 5.2: Simulation parameters for MIMO-OFDM system

Constraint length $K$	Generators in octal		$d_{\text{free}}$	Upper bound on $d_{\text{free}}$
3	5	7	5	5
4	15	17	6	6
6	53	75	8	8
7	133	171	10	10
9	561	753	12	12

Table 5.3: Rate 1/2 maximum free distance codes

# Walsh codes	$L$	$\{4, 8, 16, 32, 64, 128, 256\}$
# active users	$N_u$	$\{1, 2, \dots, L\}$

Table 5.4: Simulation parameters for MIMO MC-CDMA system

## 5.2 The Performance of MIMO-OFDM System

Figure 5.1 shows the BER performance of the MIMO-OFDM system in the two-path channel.

The convolutional encoder is specified as in Table 5.3. At high  $E_b / N_o$ , the longer constraint length  $K$  has a better BER performance. This because the free distance  $d_{\text{free}}$  of a convolutional code is proportional to the constraint length  $K$ . Our simulation result shows that

when  $K = 9$ , the BER approaches  $10^{-6}$  at  $E_b/N_o = 5\text{dB}$ . On the other hand, the encoder with shorter constraint length outperforms one with the longer constraint length at low  $E_b/N_o$ . This is because at low SNR, the error probability is no longer dominated by the free distance  $d_{\text{free}}$ .

Figure 5.2 shows the BER performance of the MIMO-OFDM system in the UMTS defined six-path channel.



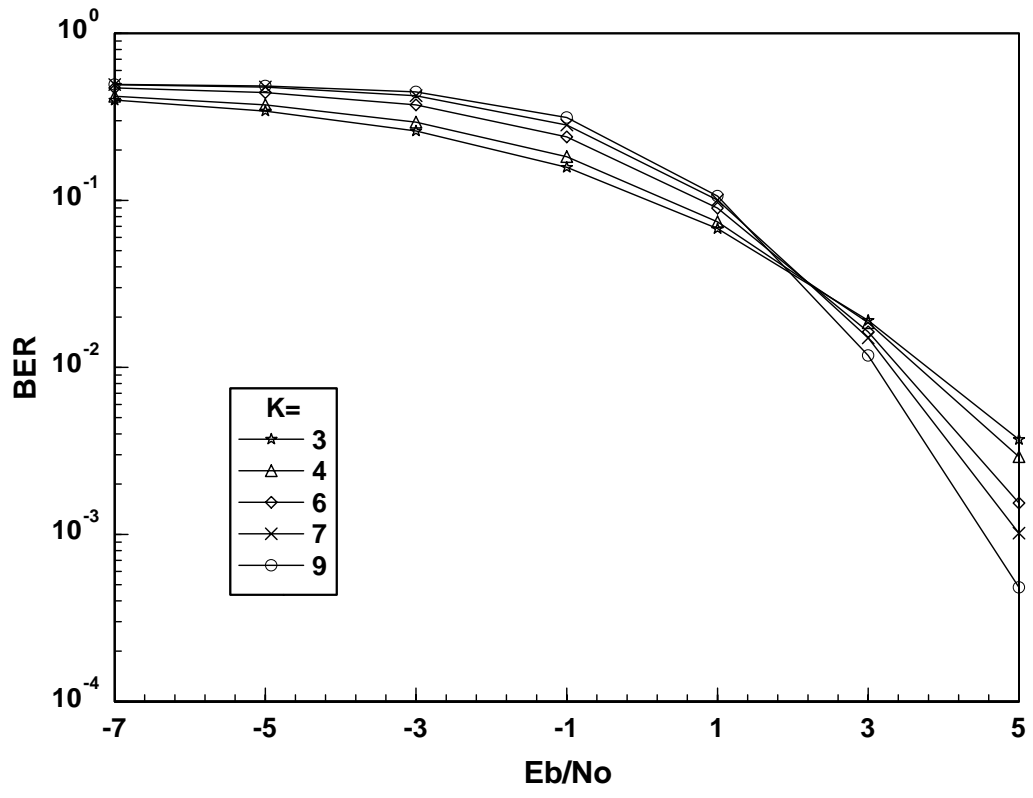


Figure 5.1: BER performance of the MIMO-OFDM system in the two-path channel

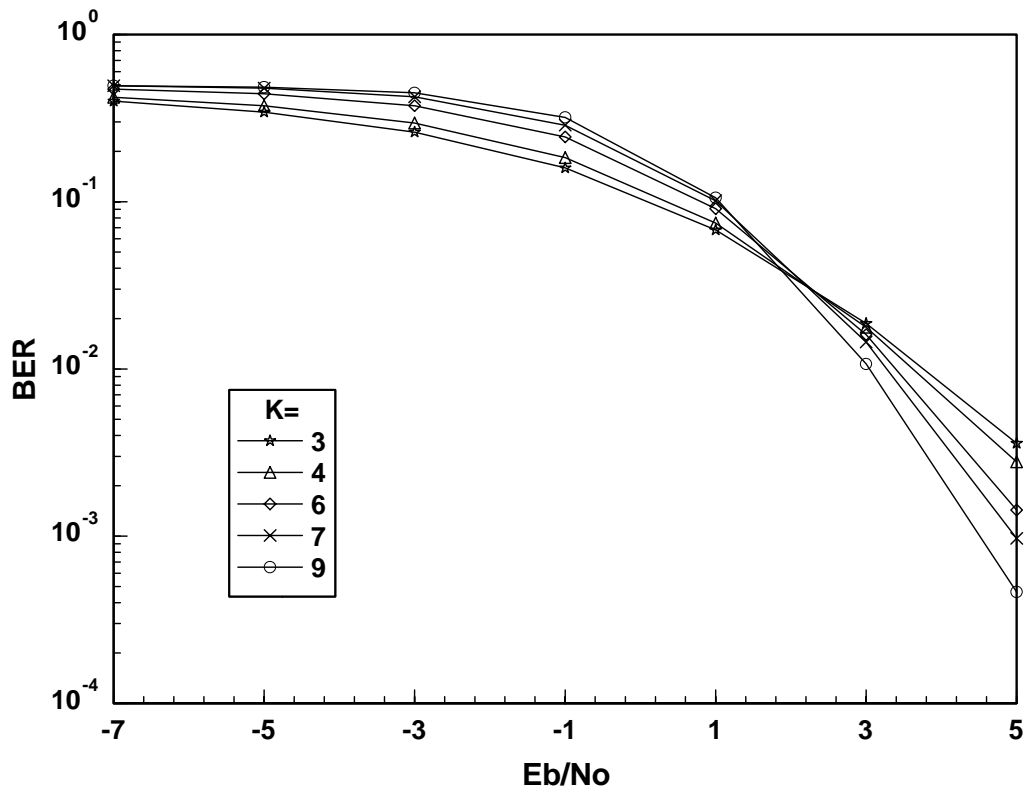


Figure 5.2: BER performance of the MIMO-OFDM system in the UMTS defined six-path channel

## 5.3 The Performance of MIMO MC-CDMA System

Figure 5.3 shows the BER performance of the MIMO MC-CDMA system in the two-path channel. The number of Walsh codes  $L$  is equal to the number of active users  $N_u = 256$ , so all the spreading codes are used ,i.e., the system is full-loaded. The BER performance for the first iteration has an error floor at  $BER=10^{-1}$  because large IAI and MPI are included. For the second iteration, the BER performance is improved by using adaptive MMSE and MPIC. This procedure is iterated several times to obtain more and more reliable data decision results. After several iterations (the 4<sup>th</sup> iteration in this case), since the adaptive MMSE cannot further improve the BER performance, MPIC is executed alone to achieve full diversity gains gradually. At which iteration the system should turn to MPIC only processing can be decided by compare the decision results between two iterations. When the MPIC decision results of the former iteration are the same as the MMSE decision results of the latter iteration for more than 90%, MPIC can then be executed only at the next and latter iterations. Our simulation results shows that after 9 iterations, the BER performance at high  $E_b / N_0$  approaches the theoretical limit and the degradation is only about 0.3 dB at  $BER = 10^{-4}$ . This simulation result shows that our iterative multi-layered detection method works well and can obtain the full benefits of both spatial diversity and path diversity.

Figure 5.4 shows the BER performance of the MIMO MC-CDMA system at all four layers in the UMTS defined six-path channel. We can see that after 9 iterations, the BER performance of the MIMO MC-CDMA system is degraded by only 0.5dB at  $BER = 10^{-4}$  as compared with the case of the perfect LAIC and MPIC.

Figure 5.5 shows the BER performance of the MIMO MC-CDMA system at all four layers in the two-path channel. Our simulations show that the  $Q$ th layered detection has a better BER performance than the  $(Q-1)$ th layered detection for the same iteration. This is because the layered detection is started with the first layer and is done in a round robin fashion. Every layer finally approaches almost the same BER performance, i.e., the iterative multi-layered detection method is not sensitive to the order of the layer processing.

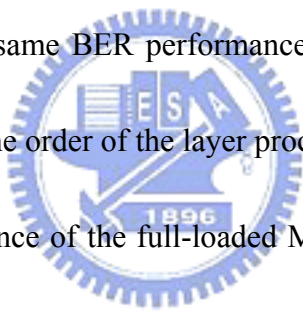


Figure 5.6 shows the BER performance of the full-loaded MIMO MC-CDMA system in the two-path channel for different spreading length  $L$ . As shown in the figure, the BER performance degrades as the spreading length  $L$  increases. This is because the longer spreading length provides the system more frequency diversity. On the other hand, the complexity also grows with the spreading length, which will be specified in the next paragraph. We can see that at the range  $L \geq 16$ , the BER degradation is not severe. Therefore,  $L = 16$  is a choice to strike a balance between system complexity and BER performance.

Figure 5.7 shows the BER performance of the half-loaded MIMO MC-CDMA system in the two-path channel for different spreading length  $L$ . We can observe that unlike the full-loaded



case which only approaches the theoretical limit of BER performance at high  $E_b / N_0$  (Figure 5.6), the half-loaded system also approaches the theoretical limit of BER performance at low  $E_b / N_0$ . The simulation results show that the BER degradation becomes severe after  $L < 16$ , which also matches to the case for full-loaded system in Figure 5.6.

Figure 5.8 shows the BER performance of the MIMO MC-CDMA system for different number of users  $N_u$  with fixed spreading length  $L = 16$ , i.e., the system load  $N_u / L$  is ranging from 1 to 1/4. We can see that the BER decreases with the value of  $N_u$ . This is because if more Walsh codes are used, more LAI and ICI will occur to received signals, hence degrade the system performance.



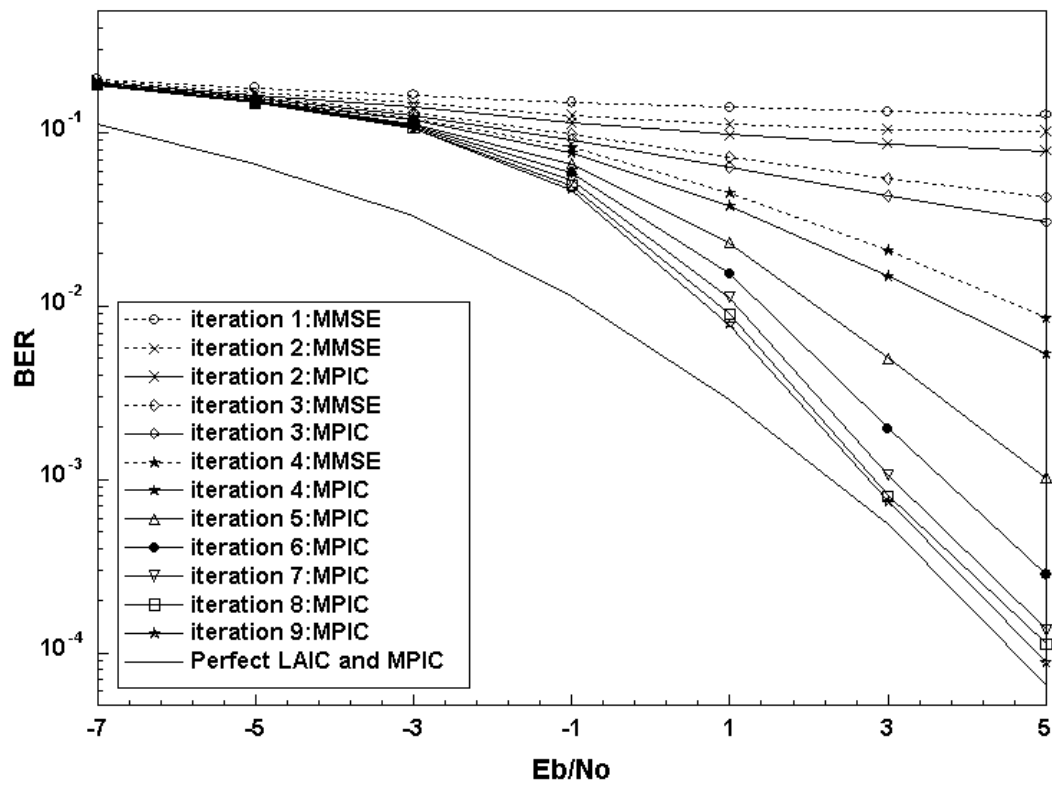


Figure 5.3: BER performance of the MIMO MC-CDMA system in the two-path channel with

$$L = N_u = 256, \text{ i.e., a full-loaded system}$$

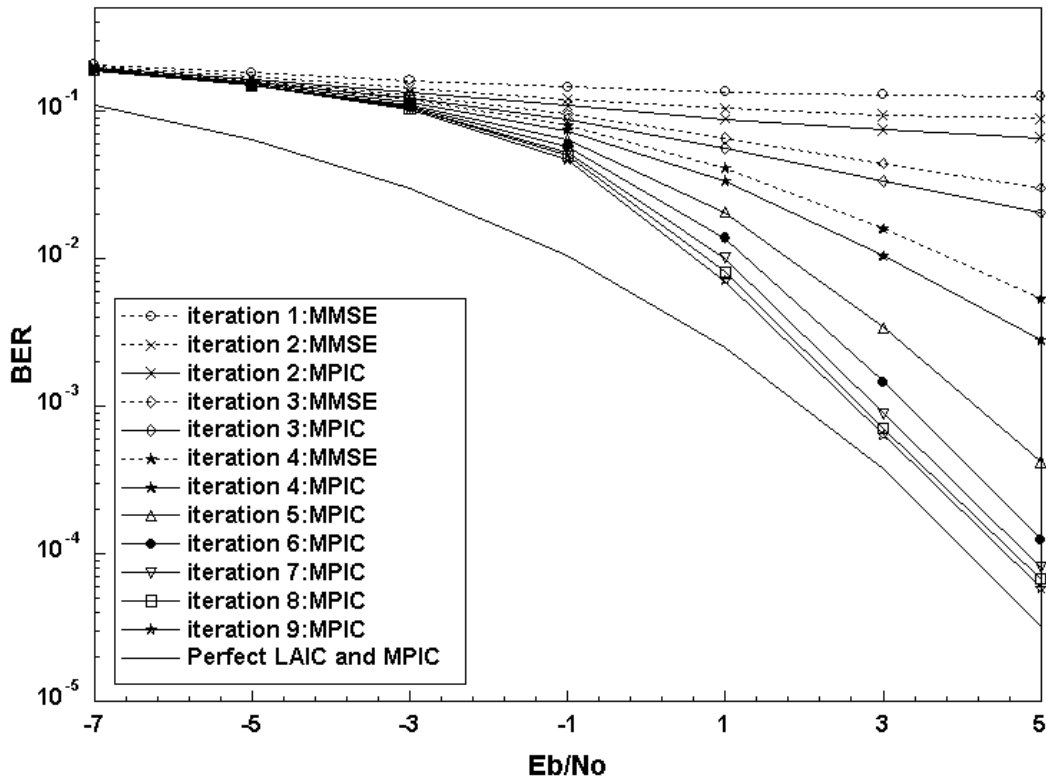


Figure 5.4: BER performance of the MIMO MC-CDMA system in the UMTS defined

six-path channel with  $L = N_u = 256$ , i.e., a full-loaded system

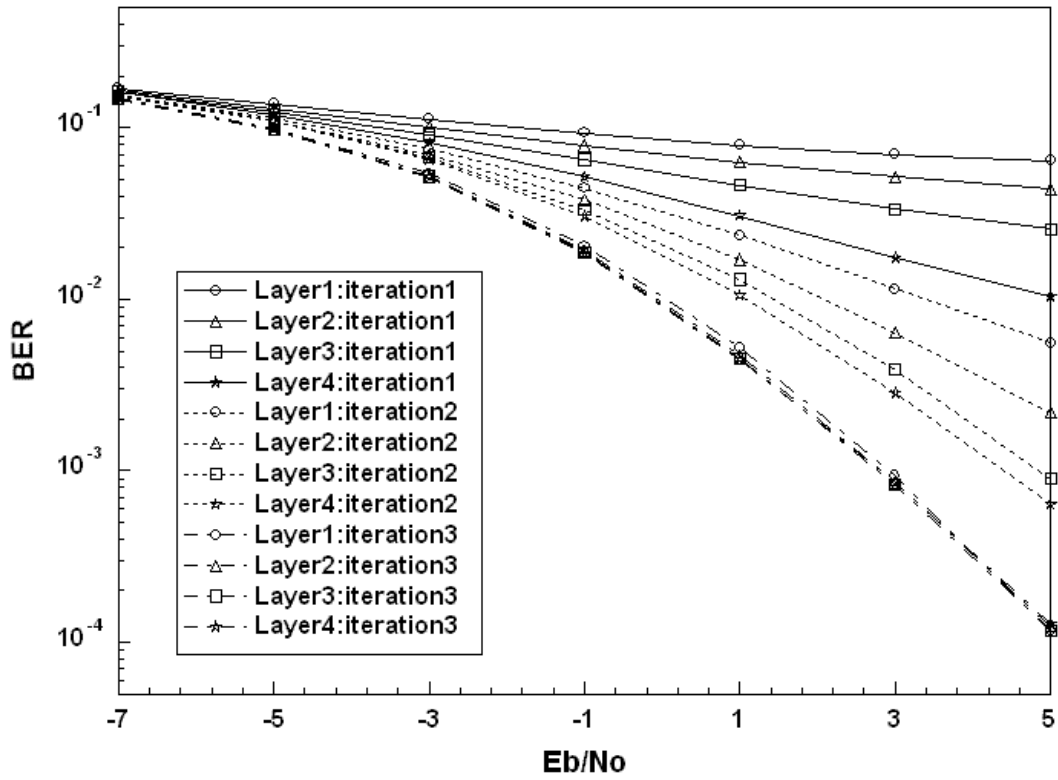


Figure 5.5: BER performance of the MIMO MC-CDMA system at all four layers in the two-path channel

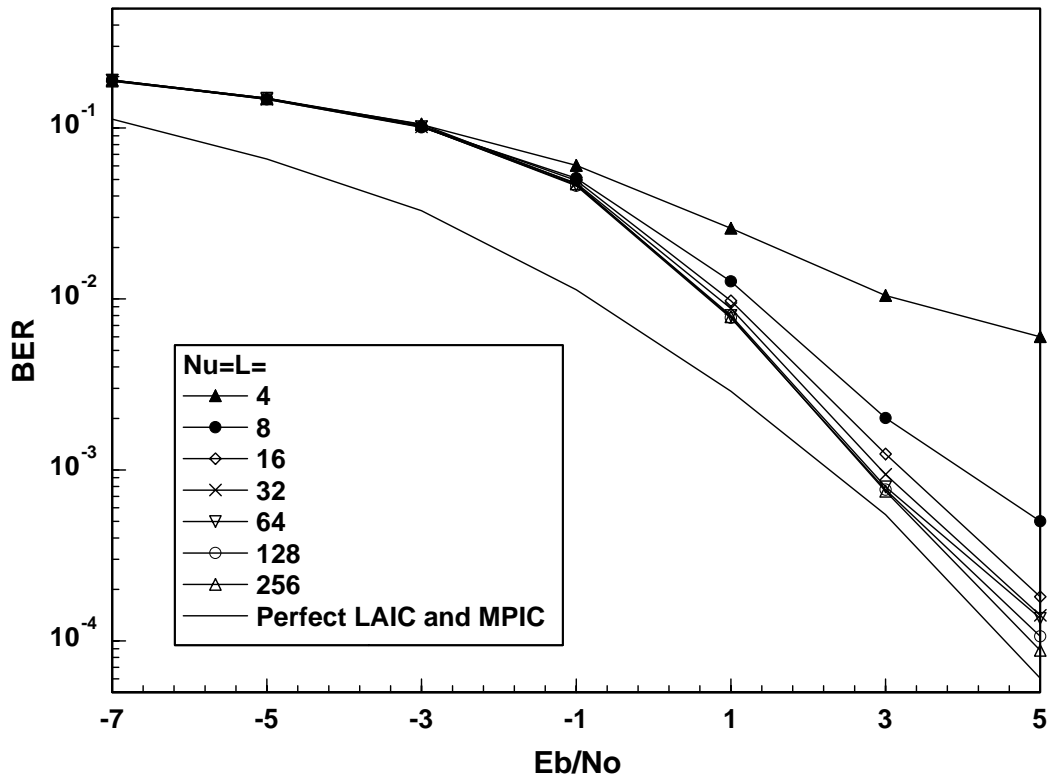


Figure 5.6: BER performance of the full-loaded MIMO MC-CDMA system in the two-path channel for different spreading length  $L$

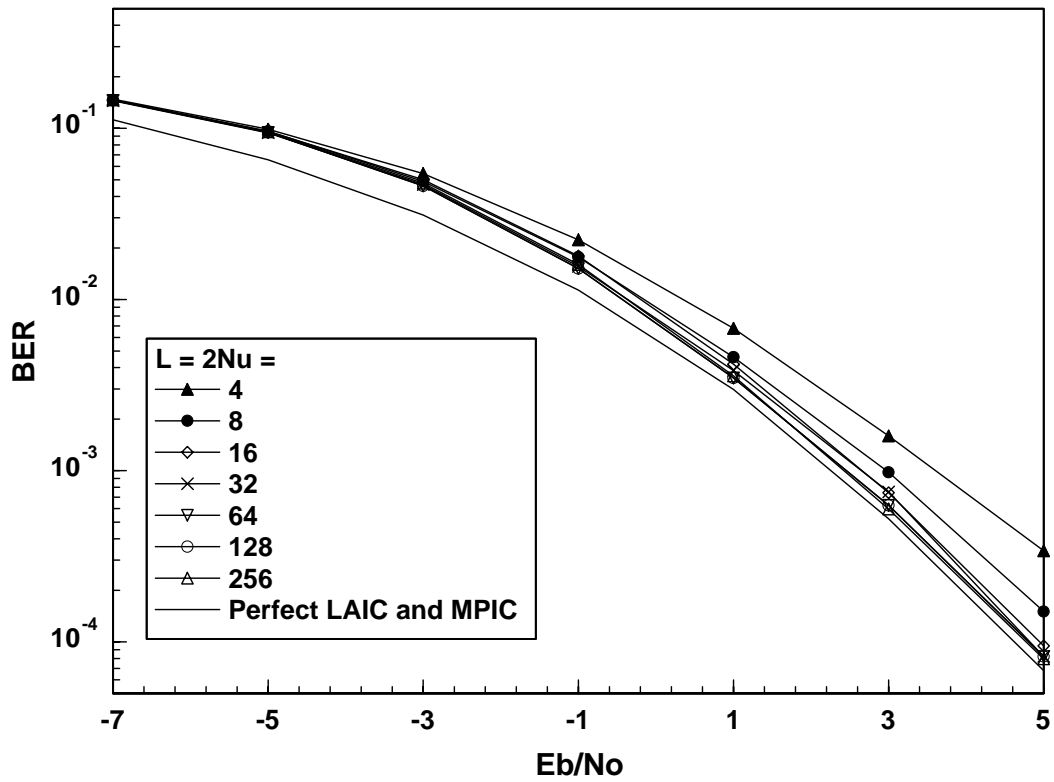


Figure 5.7: BER performance of the half-loaded MIMO MC-CDMA system in the two-path channel for different spreading length  $L$

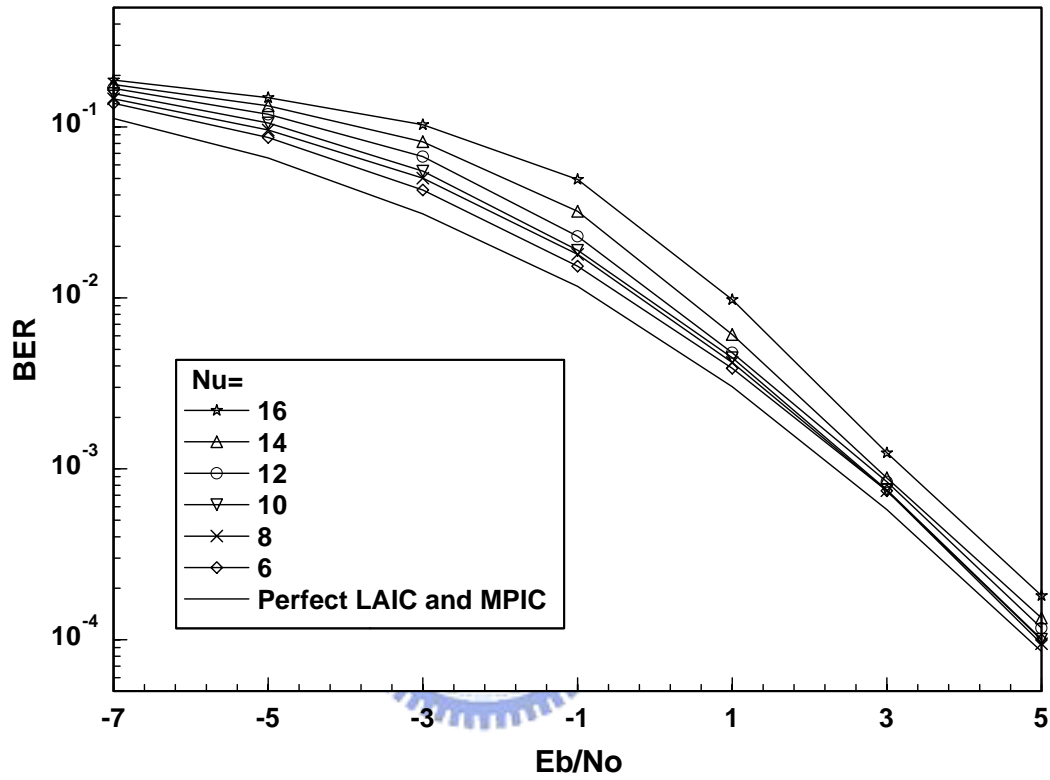


Figure 5.8: BER performance of the MIMO MC-CDMA system for different number of users

$N_u$  with fixed spreading length  $L = 16$

## 5.4 Comparison of the MIMO-OFDM and MIMO MC-CDMA systems

We compare the system performance of the MIMO-OFDM and MIMO MC-CDMA systems in this paragraph. For MIMO-OFDM systems, the convolutional encoders in Table 5.3 with rate  $1/2$  are used; and for MIMO MC-CDMA systems, we consider the case with system load  $N_u/L=1/2$ . Table 5.5 compares the complexity of the two systems. Most complexity of the MIMO-OFDM system is for decoding process. For the MIMO MC-CDMA system, spreading and despreading process are the dominant factor of the total complexity. Figure 5.9 shows the BER performance of the two types of systems. We observe that MIMO MC-CDMA systems significantly outperform MIMO-OFDM systems in the low  $E_b/N_0$  region. This is because the MPIC method for MIMO MC-CDMA systems can fully achieve diversity gains including both spatial diversity and multipath diversity. On the other hand, MIMO-OFDM systems slightly outperform MIMO MC-CDMA systems in the high  $E_b/N_0$  region. This is because the coding gain for MIMO-OFDM systems can be fully achieved when  $E_b/N_0$  is high.



Process \ System	MIMO-OFDM	MIMO MC-CDMA
Each layer:	at all receivers	at each receiver
MMSE	$4N(4M^2J + 2M^3)$	$8N + 2MN + 2$
LAIC	$4MNJ$	$2LMN + 6MN$
MPIC	0	$8NP + 4N(L + 1)$
Decoding	$MN2^K / R$	0
Total	1392640	1032224

Table 5.5: The complexity comparison of MIMO-OFDM and MIMO MC-CDMA system

(measured by the number of the real multiplier,  $K = 9$ ,  $L = 16$ ,  $P = 2$ )

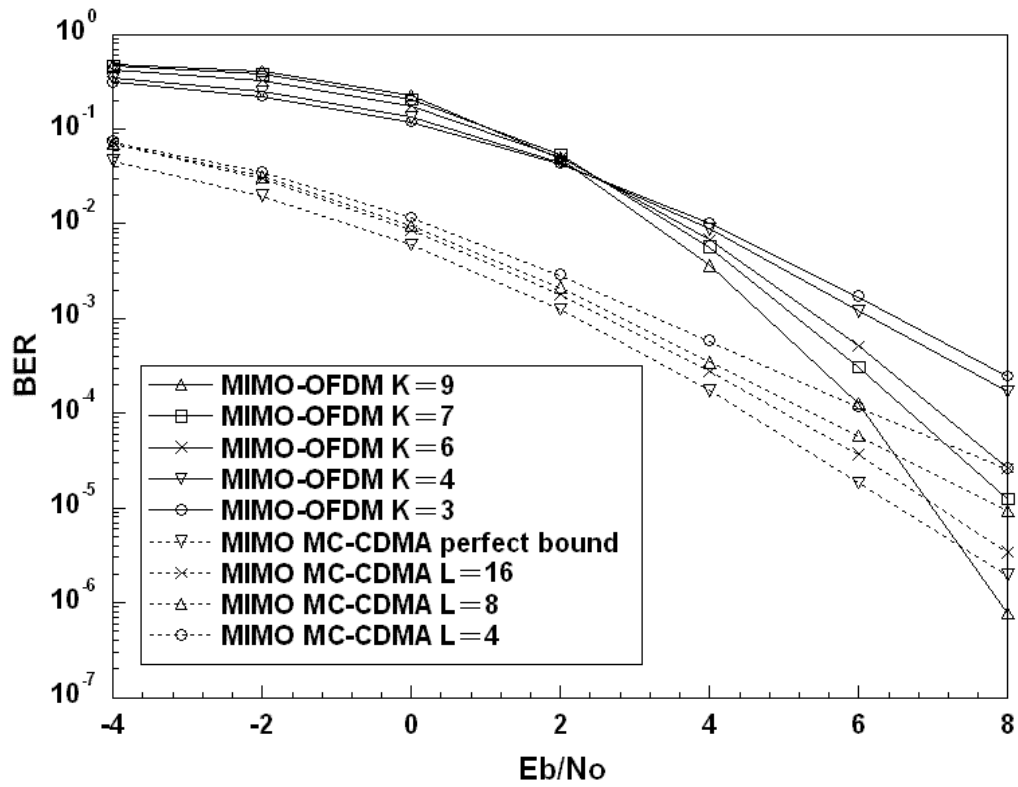


Figure 5.9: BER performance of MIMO-OFDM systems with 1/2-rate convolutional coding and half-loaded MIMO MC-CDMA systems

## 5.5 Multi-cell Environment

### 5.5.1 Gaussian Approximation

In this paragraph we discuss the BER performance of the MIMO-OFDM and MIMO MC-CDMA systems in the multi-cell environment. The model of the cellular system is as described in Figure 4.8. A simplified multi-cell environment is assumed, i.e., all interfering cells have the same and constant weighting factor  $E_i/E_0$ . In order to verify the Gaussian approximation in Eq. (4.3), Figure 5.10 and Figure 5.11 show the simulation results of the MIMO-OFDM system with code rate  $R=1/2$  and the half-loaded MIMO MC-CDMA system respectively, in a simplified multi-cell environment. The BER is plotted as a function of the difference in received power between each interfering base station and the desired base station with the number of interfering cells as a parameter. The dashed curves represent the Gaussian approximation. We can see that for both MIMO-OFDM and MIMO MC-CDMA systems the Gaussian approximation model accurately.

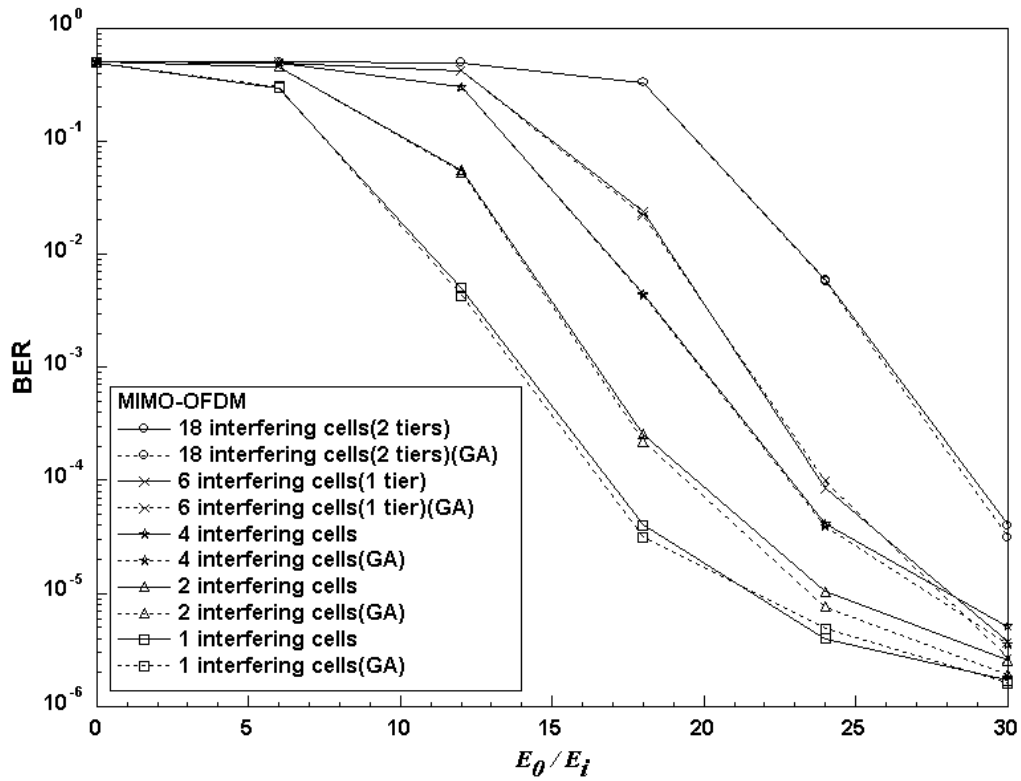


Figure 5.10: BER performance of the MIMO-OFDM system in a multi-cell environment with

code rate  $R = 1/2$ , constraint length  $K = 9$ , and  $E_b / N_0 = 8\text{dB}$

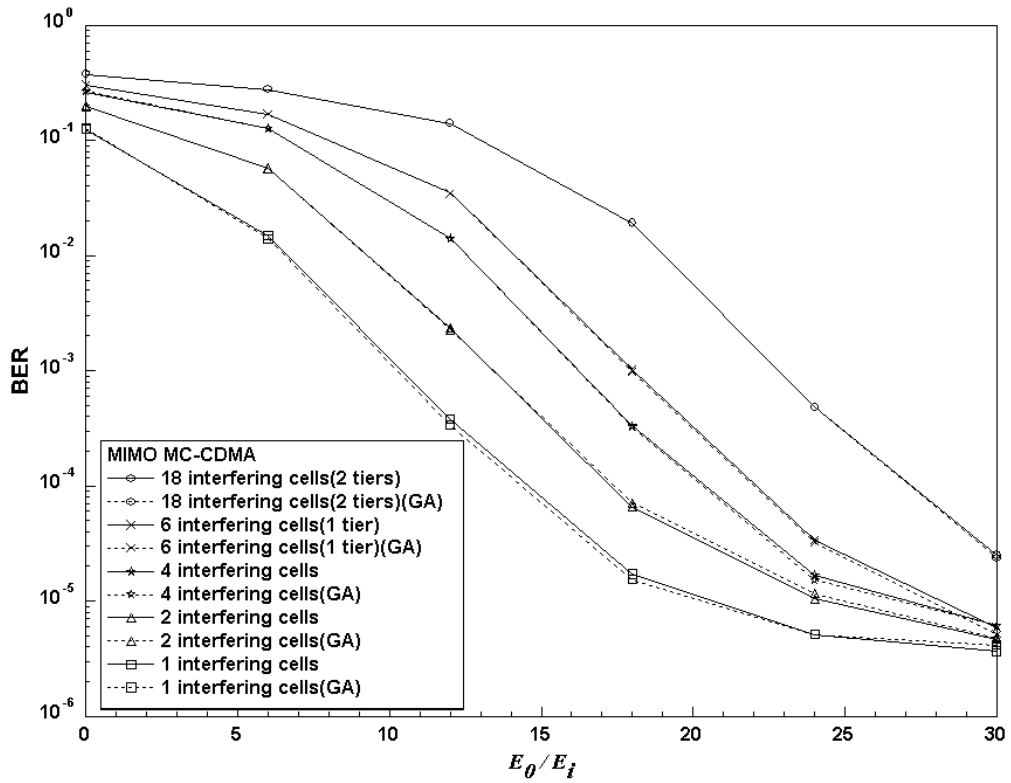
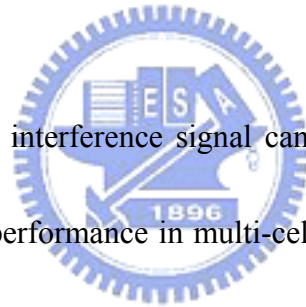


Figure 5.11: BER performance of the half-loaded MIMO MC-CDMA system in a multi-cell

environment with Walsh codes length  $L = 16$  and  $E_b/N_0 = 8\text{dB}$

## 5.5.2 Analyses of System Performance in Multi-cell Environment

In order to reduce interferences, directional antenna can be used [15]. When  $S$  (a small integer) directional antennas are used at a base station to illuminate  $S$  different sectors in a cell, the interference can be reduced by a factor of  $S$ . This reduction can be defined as sectored antenna gain  $G_s$ . Another approach for interference reduction is the relatively low speech activity factor, which is about 40% during two-way conversations [21]. This can be defined as voice activity gain  $G_v$ .



By Gaussian approximation, the interference signal can be modeled as Gaussian noise; hence the discussion of the system performance in multi-cell environment can be simplified.

It should be noticed that in our MIMO systems, the interference signal power received at each receive antenna is proportional to the number of transmit antenna  $M$ . For example, in our simulations  $M = 4$ , a -5 dB SIR is equivalent to a -11dB  $E_b/N_0$  by Gaussian approximation. Assume  $G_s = 3$  ( $S = 3$ ) and  $G_v = 2.5$  (40% voice activity), according to the simulation results of the SIR distributions in paragraph 4.2, we can obtain the simulated distribution of user's average error probability at two tiers' multi-cell environment (ignoring the effect of noise) in Figure 5.12. We can see that MIMO MC-CDMA systems outperform MIMO-OFDM systems in both downlink and uplink channels.

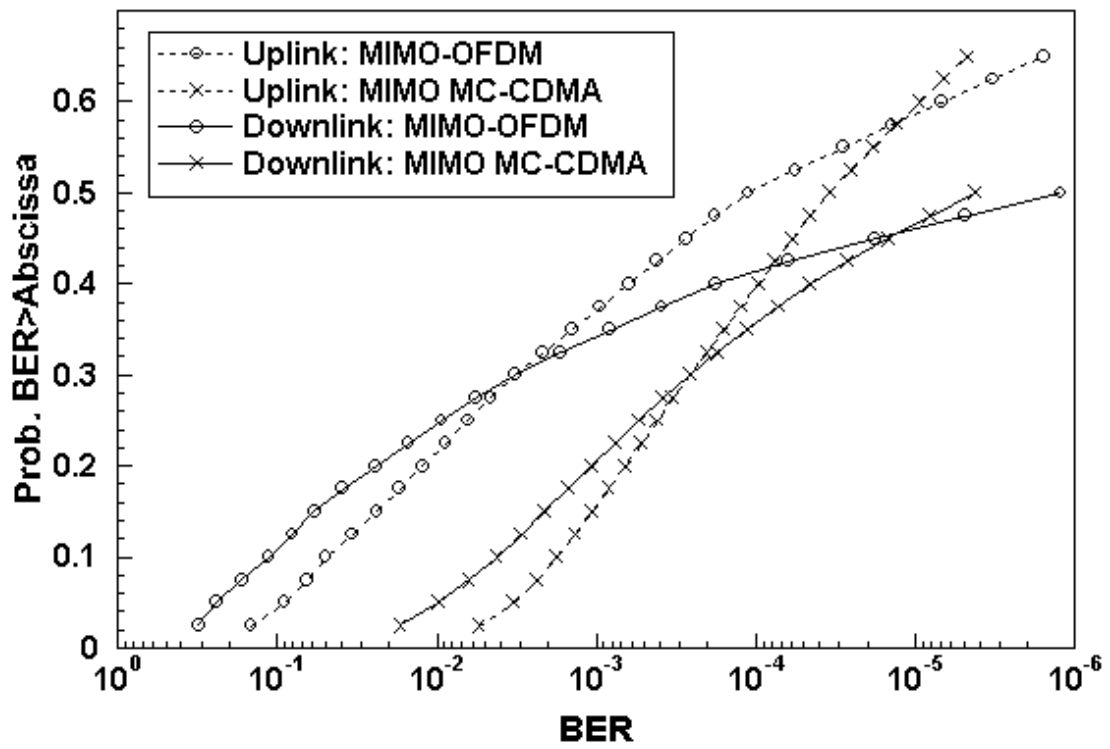


Figure 5.12: Simulated distribution of user's average error probability at two tiers' multi-cell environment

# Chapter 6

## Conclusions

High data rate and spectral efficiency is a major demand for the future generation of wireless communication systems. Many attractive candidates of transmission schemes are based on OFDM. In this paper, we conduct a comparison of the MIMO-OFDM and MIMO MC-CDMA systems. For MIMO-OFDM system, we adopt the V-BLAST detection and convolutional coding technique; for MIMO MC-CDMA system, we use an iterative multi-layered detection method combined with a MPIC technique to suppress the interference induced by multi-layered transmission and multipath environment. We observe that MIMO MC-CDMA significantly surpasses MIMO-OFDM at low SNR region. At high SNR region, MIMO-OFDM slightly outperforms MIMO MC-CDMA. In Chapter 4, a multi-cell environment is introduced hence we can extend our investigations to more realistic scenario, i.e., cellular structures. Simulations show a good match by replacing the interfering signals with the Gaussian approximation. From computer simulations of the SIR distributions we can obtain the user's average error probability in a multi-cell environment for both MIMO-OFDM



and MIMO MC-CDMA systems. Simulation results show that MIMO MC-CDMA has a better performance in a multi-cell environment.



# APPENDIX A

## The Modified MMSE V-BLAST Equalizer

Our goal is to design the equalization matrix  $\mathbf{G}$  to minimize the mean square error, namely  $E\{\|\mathbf{x} - \mathbf{G}\mathbf{z}\|^2\}$  where  $\mathbf{x}$  is the transmitted signal vector and  $\mathbf{z}$  is the received signal vector after matching in frequency domain as described in subsection 3.1. Each component of  $\mathbf{x}$  has zero mean and unit variance, i.e.,  $E\{\mathbf{x}\mathbf{x}^H\} = \mathbf{I}$ . Moreover, the vector  $\mathbf{n}$  is the noise with zero mean and variance  $\sigma_n^2$ , i.e.,  $E\{\mathbf{n}\mathbf{n}^H\} = \sigma_n^2 \mathbf{I}$ . By the principle of orthogonality, we have:

$$E\{(\mathbf{x} - \mathbf{G}\mathbf{z})\mathbf{z}^H\} = 0 \quad (\text{A-1})$$

Expand the equation, the first term becomes:

$$\begin{aligned} E\{\mathbf{x}\mathbf{z}^H\} &= E\{\mathbf{x}\mathbf{x}^H \mathbf{H}^H \mathbf{H}\} + E\{\mathbf{x}\mathbf{n}^H \mathbf{H}\} \\ &= \mathbf{H}^H \mathbf{H} \end{aligned} \quad (\text{A-2})$$

The second term becomes:

$$\begin{aligned} E\{\mathbf{G}\mathbf{z}\mathbf{z}^H\} &= \mathbf{G}E\{(\mathbf{H}^H \mathbf{H}\mathbf{x} + \mathbf{H}^H \mathbf{n})(\mathbf{x}^H \mathbf{H}^H \mathbf{H} + \mathbf{n}^H \mathbf{H})\} \\ &= \mathbf{G}(\mathbf{H}^H \mathbf{H}\mathbf{H}^H \mathbf{H} + \sigma_n^2 \mathbf{H}^H \mathbf{H}) \end{aligned} \quad (\text{A-3})$$

Thus, we obtain

$$\mathbf{G} = (\mathbf{H}^H \mathbf{H} \mathbf{H}^H \mathbf{H} + \sigma_n^2 \mathbf{H}^H \mathbf{H})^{-1} \mathbf{H}^H \mathbf{H} \quad (\text{A-4})$$



# Reference

- [1] G. J. Foschini and M. J. Gans, "On limits of wireless communications in a fading environment when using multiple antennas," *Wireless Pers. Commun.*, vol. 6, no. 3, pp. 311-335, March 1998.
- [2] E. Telatar, "Capacity of multi-antenna Gaussian channels," *European Trans. On Telecommun.*, vol. 10, no. 6, pp. 585-595, Nov./Dec. 1999.
- [3] G. Raleigh, and J. M. Cioffi, "Spatio-temporal coding for wireless communication," *IEEE Trans. Commun.*, vol. 46, no. 3, pp. 357-366, March 1998.
- [4] G.D. Golden, C.J. Foschini, R.A. Valenzuela, and P.W. Wolniansky, "Detection algorithm and initial laboratory results using V-BLAST space-time communication architecture", *Electronics Letters*, vol. 35, pp. 14 – 16, Jan. 1999.
- [5] A. C. McCormick and E. A. Al-Susa, "Multicarrier CDMA for Future Generation Mobile Communication," *IEE Journal on Electronics & Communication Engineering*, vol. 14, no. 2, pp. 52-60, Apr. 2002.
- [6] S. Hara and R. Prasad, "Design and performance of multicarrier CDMA system in frequency selective Rayleigh fading channels," *IEEE Trans. Veh. Technol.*, vol. 48, no. 5, pp. 1584–1594, Sep. 1999.
- [7] R. Kimura and E. Adachi, "Comparison of OFDM and Multicode MC-CDMA in Frequency Selective Fading Channel," *Electron. Letters*, vol. 39, no. 3, pp. 317-318, Feb. 2003.
- [8] S. Abeta, H. Atarashi, M. Sawahashi, and F. Adachi, "Performance of coherent multi-carrier/DS-SS-CDMA and MC-CDMA for broadband packet wireless access," *IEICE Trans. Commun.*, vol. E84-B, no. 3, pp. 406–414, Mar. 2001.
- [9] K. Higuchi, A. Fujiwara and M. Sawahashi, "Multipath Interference Canceller for High-Speed Packet Transmission with Adaptive Modulation and Coding Scheme in W-CDMA Forward Link," *IEEE Journal on Commun.*, vol. 20, no. 2, pp. 419-432, Feb. 2002.
- [10] N. Miki, S. Abeta, H. Atarashi and M. Sawahashi, "Multipath Interference Canceller Using Soft-Decision Replica Combined with Hybrid ARQ in W-CDMA Forward Link,"

- in *Proc. IEEE Veh. Technol. Conf.*, vol. 3, Oct. 2001, pp. 1922-1926.
- [11] T. Kawamura, K. Higuchi, Y. Kishiyama and M. Sawahashi, "Comparison Between Multipath Interference Canceller and Chip Equalizer in HSDPA in Multipath Channel," in *Proc. IEEE Veh. Technol. Conf.*, vol. 1, May 2002, pp. 459-463.
- [12] KyunByoung Ko, Dongseung Kwon, Daesoon Cho, Changeon Kang and Daesik Hong, "Performance analysis of a multistage MPIC in 16-QAM CDMA systems over multipath Rayleigh fading channels," in *Proc. IEEE Veh. Technol. Conf.*, vol. 4, April 2003, pp. 2807-2811.
- [13] P. W. Wolniansky, G. J. Foschini, G. D. Golden, R. A. Valenzuela, "V-BLAST: An Architecture for Realizing Very High Data Rates Over the Rich-Scattering Wireless Channel," in *Proc. Int. Symp. Signals, Systems, and Electronics (ISSSE'98)*, Pisa, Italy, Oct. 1998, pp. 295-300.
- [14] Ching-Kai Li, "A novel iterative multi-layered detection method for MIMO multi-code multicarrier systems", M.S. Thesis, Dept. Com. Eng., NCTU, Hsinchu, ROC, 2005.
- [15] William C.Y Lee. *Mobile Cellular Telecommunications Systems*, McGraw-Hill Book Company, 1989.
- [16] A. J. Viterbi, A. M. Viterbi, and E. Zehavi, "Other-cell interference in cellular power-controlled CDMA," *IEEE Transactions on Communications*, vol. 42, no. 21314, pp. 1501-1504. February/March/April 1994.
- [17] Chia-Chi Huang, "Computer simulation of a direct sequence spread spectrum cellular radio architecture," *IEEE Trans. Veh. Technol.*, vol. 41, pp. 554-550, Nov. 1992.
- [18] K. Gilhousen, I. Jacobs, R. Padovani, A. Viterbi, L. Weaver, and C. Wheatley, "On the capacity of a cellular CDMA system: *IEEE Transactions on Vehicular Technology*, vol. 40, no. 2, pp. 303-312. May 1991.
- [19] Jonathan P. Castro, "The UMTS network and radio access technology: air interference techniques for future mobile systems," *New York: Wiley*, 2001.
- [20] John G. Proakis, *Digital Communications*, Mc-Graw Hill, 4th ed., 2001.
- [21] P. T. Brady, "A statistical analysis of on-off patterns in 16 conversations," *Bell System Tech. J.*, pp. 73-91, Jan. 1968.